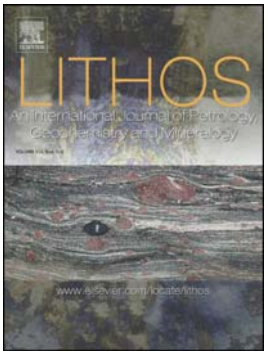

Trace element composition of silicate inclusions in sub-lithospheric diamonds from the juina-5 kimberlite: Evidence for diamond growth from slab melts

A.R. Thomson, S.C. Kohn, G.P. Bulanova, C.B. Smith, D. Araujo, M.J. Walter

PII: S0024-4937(16)30264-X
DOI: doi: 10.1016/j.lithos.2016.08.035
Reference: LITHOS 4054

To appear in: *LITHOS*

Received date: 15 March 2016
Revised date: 19 August 2016
Accepted date: 25 August 2016

Please cite this article as: Thomson, A.R., Kohn, S.C., Bulanova, G.P., Smith, C.B., Araujo, D., Walter, M.J., Trace element composition of silicate inclusions in sub-lithospheric diamonds from the juina-5 kimberlite: Evidence for diamond growth from slab melts, *LITHOS* (2016), doi: 10.1016/j.lithos.2016.08.035

TRACE ELEMENT COMPOSITION OF SILICATE INCLUSIONS IN SUB-LITHOSPHERIC DIAMONDS FROM THE JUINA-5 KIMBERLITE: EVIDENCE FOR DIAMOND GROWTH FROM SLAB MELTS.

A.R. Thomson[1,2*], S.C. Kohn[2], G.P. Bulanova[2], C.B. Smith[2], D. Araujo[3] and M.J. Walter[2]

[1]*present address, Department of Earth Sciences, University College London, London, WC1E 6BT.*

[2]*School of Earth Sciences, University of Bristol, Wills Memorial Building, Queens's Road, Bristol, BS8 1RJ.*

[3]*present address, Rio Tinto Exploration Pty. Limited, 1 Research Avenue, Bundoora, VIC 3083, Australia*

Corresponding Author (a.r.thomson@ucl.ac.uk)

ABSTRACT

The trace element compositions of inclusions in sub-lithospheric diamonds from the Juina-5 kimberlite, Brazil, are presented. Literature data for mineral/melt partition coefficients were collated, refitted and employed to interpret inclusion compositions. As part of this process an updated empirical model for predicting the partitioning behaviour of trivalent cations for garnet-melt equilibrium calibrated using data from 73 garnet-melt pairs is presented. High levels of trace element enrichment in inclusions interpreted as former calcium silicate perovskite and majoritic garnet preclude their origin as fragments of an ambient deep mantle assemblage. Inclusions believed to represent former bridgmanite minerals also display a modest degree of enrichment relative to mantle phases. The trace element composition of 'NAL' and 'CF phase' minerals are also reported. Negative Eu, Ce, and Y/Ho anomalies alongside depletions of Sr, Hf and Zr in many inclusions are suggestive of formation from a low-degree carbonatitic melt of subducted oceanic crust. Observed enrichments in garnet and 'calcium perovskite' inclusions limit depths of melting to less than ~ 600 km, prior to calcium perovskite saturation in subducting assemblages. Less enriched inclusions in sub-lithospheric diamonds from other global localities may represent deeper diamond formation. Modelled source rock compositions that are capable of producing melts in equilibrium with Juina-5 'calcium perovskite' and majorite inclusions are consistent with subducted MORB. Global majorite inclusion compositions suggest a common process is responsible for the formation of many superdeep diamonds, irrespective of geographic locality. Global transition zone inclusion compositions are reproduced by fractional crystallisation from a single parent melt, suggesting that they record the crystallisation sequence and melt evolution during this interaction of slab melts with ambient mantle. All observations are consistent with the previous hypothesis that many superdeep diamonds are created as slab-derived carbonatites interact with peridotitic mantle in the transition zone.

Keywords: sub-lithospheric diamonds, trace elements, melts, subduction, transition zone, carbon cycle

HIGHLIGHTS

- The trace element composition of inclusions in sub-lithospheric diamonds from the Juina-5 kimberlite are reported
- An updated empirical model for the partitioning of trivalent cations between garnet and melt is presented
- High levels of enrichment, Ce, Eu and Y/Ho anomalies and depletions of Zr, Hf and Sr observed in Juina-5 inclusions demonstrate they crystallised from slab-derived melts
- Global transition zone inclusions appear to record the fractional crystallisation sequence of slab melts

1. INTRODUCTION

Diamonds, and the mineral inclusions they trap during growth, are pristine samples from the mantle that reveal processes in the deep Earth. Whilst the majority of diamonds originated in the lithosphere (Stachel et al., 2005) some, known as sub-lithospheric or superdeep diamonds, have been exhumed from asthenospheric depths extending throughout the transition zone and into the lower mantle (see Harte, 2010 for a recent review). Such samples provide a unique insight into mantle geodynamics on a small length-scale that is highly complementary to spatial information gained using seismic techniques (e.g. Chang et al., 2015).

Studies of superdeep diamonds have generally categorised samples by associating observed inclusion assemblages with paragenesis in either ultrabasic (metaperidotite) or basic (metabasite or eclogitic) protoliths. Mostly these associations, or 'mineral facies', have been defined by comparing the observed inclusion mineralogies with experimental phase diagrams for high pressure pyrolite or eclogite bulk compositions (e.g. Harte, 2010). Using this approach, diamonds containing inclusions of $MgSiO_3$, and/or $CaSiO_3$ coexisting with (Mg,Fe)O are categorised as ultrabasic lower mantle samples (e.g. Davies et al., 2004a; Harte et al., 1999; Hayman et al., 2005; Stachel et al., 2000b), whereas those containing $(Mg,Fe)(Si,Al)O_3$, $Ca(Si,Ti)O_3$, SiO_2 and $(Na,K)(Mg,Fe)_2Al_5SiO_{12}$ inclusions would be described as lower mantle metabasite (e.g. Thomson et al., 2014; Walter et al., 2011). For samples containing garnet inclusions, diamond paragenesis has commonly been categorised as metaperidotitic (either harzburgitic or lherzolitic) or metabasic, primarily on the basis of CaO and Cr_2O_3 contents (e.g. Bulanova et al., 2010; Stachel, 2001; Stachel et al., 2000a). Diamonds containing inclusions of olivine stoichiometry have always been associated with metaperidotite bulk compositions. However, inclusions that do not fit neatly into either association have been observed, which led to the expansion and creation of the 'carbonatitic' (Kaminsky, 2012) and/or 'Ca-rich' association (Brenker et al., 2005; Harte and Richardson, 2012; Zedgenizov et al., 2014).

It has been widely recognised that major element compositions of many sub-lithospheric inclusions do not match those expected from experiments on mantle or subducted protoliths, and that some degree of melt metasomatism likely occurred during their formation in order to explain this mismatch (e.g. Bulanova et al., 2010; Harte, 2010; Harte et al., 1999; Harte and Hudson, 2013; Moore et al., 1991; Stachel et al., 2000a; Thomson et al., 2014; Walter et al., 2011; 2008). For instance, Stachel et al. (2000b) invoke at least one episode of metasomatism "associated with carbonatites" to explain the enrichment of LREE coupled with Ba and Nb depletions observed in Ca-rich majoritic garnet inclusions in Kankan diamonds. Walter et al. (2008) interpreted the extreme enrichment of

calcium silicate inclusions (interpreted as former perovskite) as an indication they crystallised from a "low-degree, primary carbonatite melt derived from deeply subducted crust", rather than trapped fragments of the ambient subsolidus mantle. Harte (2010) also suggested a similar model of diamond growth from slab fluids or melts based on the coincidental relationship between diamond inclusion abundance and the depths of expected dehydration reactions.

Unfortunately, the general idea that diamond-hosted inclusions are in some way representative fragments of the pristine ambient deep mantle persists (e.g. Kaminsky, 2012). Amongst other implications, it has followed from this approach that the presence of ferropericlase in diamonds has been interpreted as evidence for a lower mantle paragenesis (e.g. Davies et al., 2004b; Harte et al., 1994; Hayman et al., 2005; Hutchison, 1997; Kaminsky, 2012; Kaminsky et al., 2009a; 2001; 2015; 2009b; Wilding, 1990). Close comparison of inclusion and experimental ferropericlase compositions in specific cases have led to the interpretation that diamonds have been exhumed from depths spanning the entire lower mantle, including the D'' layer above the core-mantle-boundary (e.g. Hayman et al., 2005; Wirth et al., 2014). However, both natural samples (Kopylova et al., 1997; Stachel et al., 2000b) and experiments (Brey et al., 2004; Thomson et al., 2016) demonstrate the stability of ferropericlase with a range of compositions in equilibrium with diamond throughout the upper mantle in regions of low silica activity.

Kiseeva et al. (2016; 2013b) and Thomson et al. (2016) have recently demonstrated that many diamond-hosted majoritic garnet inclusions are neither ultrabasic or basic endmembers, despite their assignments based on CaO and Cr_2O_3 contents. Rather, they span a continuous compositional spectrum, and many samples have intermediate compositions. Whilst this could be evidence for a large reservoir of pyroxenite within the transition zone (Kiseeva et al., 2013b), it is more likely to be the consequence of interaction between metabasic and ambient mantle components (Thomson et al., 2016; Kiseeva et al., 2016). Indeed, experiments demonstrate that intermediate garnet chemistries, similar to inclusions, are generated during the reaction of MORB-derived carbonatite melts with ambient peridotite (Thomson et al., 2016). Slab-derived carbonatite melts are expected at transition zone conditions because the majority of subduction geotherms intersect a deep depression in the solidus of carbonated MORB between 400 and 600 km depth (Thomson et al., 2016). The chemical characteristics of 'calcium silicate perovskite' and ferropericlase inclusions were also reproduced by slab melt – mantle interactions. The role of subducted material in sub-lithospheric diamond formation is confirmed by their carbon and oxygen isotopic composition. Diamonds with light $\delta^{13}C$ and inclusions with heavy $\delta^{18}O$ values from Jagersfontein (Ickert et al., 2015), Juina-5,

Collier-4 and Machado River (Burnham et al., 2015b) provide unambiguous evidence of recycled crustal material. Additionally, the covariance of carbon and oxygen isotopic compositions between crustal and mantle reservoirs suggest diamond formation occurred during interaction of crustal- and mantle-derived sources (Burnham et al., 2015b). Thus, the melting of subducted oceanic crust and subsequent reaction of melts with the overlying mantle provides a unified petrological framework for explaining the generation of diamonds, their inclusion assemblages and isotopic signatures. The weight of evidence in support of such a model means that interpreting diamond inclusions as representative fragments of endmember mantle lithologies (e.g. primitive mantle peridotite or subducted MORB) is a fundamentally flawed approach and should be abandoned. In contrast, that data indicate that inclusions should be considered to represent different stages of a continuous chemical spectrum produced during interaction of recycled and mantle lithologies, often facilitated by the presence of a low-degree melt or fluid.

This study examines the trace element chemistry of silicate inclusions in sub-lithospheric diamonds to evaluate whether their observed compositions are consistent with this reaction model of superdeep diamond formation. Trace element composition of mineral inclusions from Juina-5 diamonds previously studied by Walter et al. (2011) and Thomson et al. (2014) are presented. In these studies, the diamonds were polished from one direction on a jeweller's wheel to expose one or more mineral inclusion on a flat surface, suitable for multiple types of analysis. Wavelength dispersive electron microprobe analysis was used to measure the major element chemistry of the inclusions, which was used to interpret their current and former mineralogy. The major element compositions of all inclusions studied here can be found in Walter et al. (2011) and Thomson et al. (2014). The carbon isotopic composition of the host diamonds was measured in several locations on each diamond by secondary ionisation mass spectrometery (SIMS), and are presented in Thomson et al. (2014). The inclusions in Juina-5 diamonds indicate exhumation from transition zone and/or lower mantle depths. Many composite inclusions, interpreted as former calcium silicate perovskite ($Ca[Si,Ti]O_3$ stoichiometry), bridgmanite, NAL phase, CF phase and stishovite alongside inclusions of partially re-equilibrated majoritic garnet are studied. The host diamonds dominantly have light $\delta^{13}C$ values (Thomson et al., 2014), and inclusions have heavy $\delta^{18}O$ values (Burnham et al., 2015b), suggestive of crustal material. This sample suite is ideal for examining whether the trace element abundances observed in the inclusions are consistent with formation involving melts of recycled crust. Additionally, literature data has been compiled for the trace element compositions of majoritic garnet and former 'calcium silicate perovskite' inclusions in order to evaluate whether the melt

model of diamond formation can be generalised to global sub-lithospheric diamonds containing these inclusion types, or whether this process is specific to certain localities.

2. METHODS

2.1 SIMS ANALYSES

The trace element composition of 23 mineral inclusions in 22 diamonds from the Juina-5 kimberlite in Brazil, were measured using SIMS. The samples were carefully cleaned following previous work, pressed flat into indium mounts and gold-coated for SIMS analyses using the Cameca IMS-4f microprobe at the Edinburgh Ion Microprobe Facility. For analyses a primary beam of $^{16}O^-$ ions accelerated at ~ 11 keV (net 15 keV at the sample surface) was used with a sample current of ~ 2 nA to achieve an analysis spot of ~ 15 µm at the sample surface. Molecular ion transmission was reduced using a secondary ion accelerating voltage of 4500 V, offset by 75 eV. Analyses were performed in two consecutive routines containing the 'light' and 'heavy' elements respectively. Instrumental limitations prevented all desired elements being measured in one sweep. In each routine five sweeps of the desired masses were conducted, with the spectrometer position for each element manually adjusted during the first sweep of each sample. Several elements were analysed in both routines to ensure they were internally consistent. The data were reduced using custom in house software.

Most of the Juina-5 samples are composite inclusions and consist of multiple component mineral phases. As far as practical, inclusions were analysed using a spot size to enclose the entire inclusion in order to achieve a 'bulk analysis', however some of the inclusions were too large to be analysed by a single spot. In these cases, multiple analyses were performed to assess the heterogeneity of the inclusions. Heterogeneity was also observed as a function of 'depth' in some inclusions, which is a consequence of changing proportions of coexisting composite phases beneath the inclusion surface. This was recorded by changing count rates between sequential mass sweeps.

Calibration was performed using the silicate glass standard srm610 under identical operating conditions, as in similar previous studies (Bulanova et al., 2010; Walter et al., 2008). Precision is thought to be 10 % for all isotopes. Accuracy is < 10 % relative for REE, Ba, Sr, Nb, Zr and Y. Accuracy of Hf, Rb, Th and U is within 30 % relative (R. Hinton, personal communication). Background levels were estimated by counting on mass 130.5 (where there are no measured isotopes); all analyses falling below these levels were excluded. Unfortunately, our analytical session came near the end of a detectors life cycle, thus backgrounds were higher than normally achieved using SIMS. To improve detection limits for some inclusions, a second analytical session was performed after the detector

had been replaced. Data collected were normalised using the SiO_2 content of each inclusion, as reported by Thomson et al. (2014).

2.2 Mineral/melt partition coefficients

To allow interpretation and modelling of inclusion compositions, mineral/melt partition coefficients ($D_i^{min/melt}$) are required. For some of the mineral phases of interest, e.g. bridgmanite (Corgne et al., 2005; Hirose et al., 2004; Taura et al., 2001; Walter et al., 2004; Liebske et al., 2005) and calcium silicate perovskite (Corgne and Wood, 2005; 2002; Dalou et al., 2009; Hirose et al., 2004), there are a handful of experimental studies that report $D_i^{min/melt}$, whereas there are no reported partition coefficients for NAL and/or CF phase. In contrast, many studies have investigated how trace elements partition between garnet and melt, allowing the effects of garnet chemistry, pressure and temperature on $D_i^{min/melt}$ to be evaluated (e.g. van Westrenen and Draper, 2007). In order that the most appropriate suite of partition coefficients is used in this study we have collated and evaluated all experimental data from the published literature for $D_i^{min/melt}$ in bridgmanite, calcium silicate perovskite and garnet (supplementary information). Data for trivalent (REE + Y + Sc) and quadrivalent (Th + U + Zr + Hf + Ti) cations from each literature experiment were fitted using a lattice strain model (Blundy and Wood, 1994). Fits were achieved using a Levenberg-Marquardt routine employed in MATLAB to determine D_0, r_0 and E (equation 1), assuming the ionic radii for each element (r_i) in 8-fold coordination (Shannon, 1976). The lattice strain model relates the partition coefficient of element i (D_i) with ionic radius r_i to that of element o (D_0), where the latter has the ionic radius of the crystallographic site size (r_0). E is the Young's Modulus of the site, N_A is Avogadro's number, R is the gas constant and T is the temperature in K.

$$D_i(P,T,X) = D_0(P,T,X) \times exp\left[\frac{-4\pi E N_A\left[\frac{r_0}{2}(r_i-r_0)^2+\frac{1}{3}(r_i-r_0)^3\right]}{RT}\right] \quad \text{(eq. 1)}$$

In general, the lattice strain model produces good fits to the experimental data. In a few cases there is evidence of disequilibrium or large uncertainties in experimental partition coefficients, especially for the LREE in garnet and bridgmanite, which are the largest, the slowest diffusing and the least abundant cations (Shannon, 1976; van Orman et al., 2002). The results for bridgmanite and calcium perovskite reveal some scatter between different studies that is partially explained by variations in mineral chemistry, but much of which is assumed to be caused by experimental and analytical uncertainties. Rather than simply choosing the results of one study over the others with little justification, subsets of the experimental data for bridgmanite and calcium silicate perovskite were combined and refitted. This process should reduce the uncertainty in partition coefficients by

increasing the quantity of data used for fitting. For bridgmanite all the experimental data from Walter et al. (2004) and Corgne et al. (2005) for trivalent and quadrivalent cations were combined and fitted with lattice strain parabola at a temperature of 2300 °C (figure 1). Data from Liebske et al. (2005) weren't included in this fit because their bulk compositions have elevated Al_2O_3 contents, which increase partition coefficients, compared with an ambient peridotitic mantle composition. The model partition coefficients for the LREE are lower than any of the individual analyses, which is believed to be the consequence of disequilibrium and low abundances of these elements in the experiments. Similarly, for calcium silicate perovskite, data from the 20 GPa experiments of Dalou et al. (2009) and unpublished data from LS Armstrong, S Keshav and MJ Walter were combined and fitted for 3+ and 4+ cations at 1600 °C (figure 2). Data for $CaSiO_3$ from both experiments of Corgne et al. (2002) were fitted individually, and the average of both partition coefficient sets used for modelling subsolidus peridotite. Partition coefficients for the remaining elements (Rb, Ba, Li, Nb, Ta and Sr) were assumed to be the average of measured values from the same literature experiments used in lattice strain models.

Whilst the literature data for bridgmanite and calcium silicate perovskite are insufficient to investigate the effects of composition, pressure and temperature on partition coefficients, this is not the case for garnet. Data from 73 garnet-containing experiments were collated (Bennett et al., 2004; Bobrov et al., 2014; Corgne et al., 2012; Corgne and Wood, 2005; Dalou et al., 2009; Dasgupta et al., 2009; Draper et al., 2006; Dwarzski et al., 2006; Grassi et al., 2012; Hauri et al., 1994; Klemme et al., 2002; Pertermann et al., 2004; Salters et al., 2002; Suzuki et al., 2012; Tuff and Gibson, 2007; van Westrenen et al., 1999; 2000; Walter et al., 2004) and fitted the data for trivalent cations from each dataset using lattice strain models (experimental literature data available as a supplementary file). Whilst there are previous studies that have published models predicting the individual effects of composition, pressure and temperature on D_0, r_0 and E for trivalent cations (Draper and van Westrenen, 2007; Sun and Liang, 2013; van Westrenen et al., 1999; van Westrenen and Draper, 2007; van Westrenen et al., 2001) this dataset incorporates experimental data that were not available at the time of these models. As much of the additional data are particularly applicable to Na-bearing garnets from sub-lithospheric pressures we have modified the model of van Westrenen et al. (2007) to allow prediction of D_0, r_0 and E for trivalent cations for any garnet composition at known pressure and temperature conditions. As D_0, r_0 and E are highly correlated with one another, instead of fitting each literature dataset for all three variables simultaneously a predictive model was employed to estimate E (van Westrenen and Draper, 2007), adding a term for the Na content of garnet (X_{Na} = 0.5*[Na+K], where Na and K are calculated per formula unit with 12 oxygens) to equation 3

(equations 2 and 3). The coefficient of X_{Na} was estimated based on the size of the $Na_2MgSi_5O_{12}$ garnet X-site (Bindi et al., 2011). This predicted value of *E* is used to fit the experimental data for D_0 and r_0 using equation 1, thus reducing some of the spurious scatter in fitted D_0 values.

$$E(\mathrm{GPa}) = 1826(1.38 + r_0)^{-3} + 12.4P - 0.072T + 237(\mathrm{Al} + \mathrm{Cr})_{apfu} \quad \text{(eq. 2 - van Westrenen et al., 2007)}$$

$$r_0(REE, \text{Å}) = 0.9302X_{Py} + 0.993X_{Gr} + 0.916X_{Alm} + 0.946X_{Spes} + 1.05(X_{And} + X_{Uv}) + 0.914X_{Na} - 0.0044(P - 3) + 0.000058(T - 1818) \quad \text{(eq. 3 – modified from van Westrenen et al., 2007)}$$

Blundy et al. (1995) demonstrated that D_0 is related to the enthalpy of fusion of the mineral of interest, in this case garnet, along its own melting curve. Following the same logic as presented in Blundy et al. (1995) equation 4 was simplified and fitted to the experimental dataset, providing a new empirical model for the prediction of D_0 (equation 5).

$$\Delta H^\circ_T - T\Delta S^\circ_T + P\Delta V - \frac{1}{2}\left(\frac{\partial \Delta V}{\partial P}\right)P^2 = RT\ln D_0 \quad \text{(eq. 4)}$$

$$\ln D_0 = \frac{9193 - 301.9P + 12.64P^2}{T} - 2.874 \text{ (eq. 5)}$$

Four extreme outlying data corresponding to low temperature experiments were excluded from this fit. Figure 3 plots the predicted values of D_0 using equation 5 against those from the lattice strain fitting. Later in this manuscript, when modelling the composition of individual majoritic garnet inclusions, equations 2, 3 and 5 were used to produce inclusion-specific partition coefficients. Otherwise, fits to experiment M932 (Corgne et al., 2012) or U238 (Suzuki et al., 2012) with D_o^{3+} determined using equation 5 (T = 1600 °C) were used as garnet partition coefficients in peridotitic and metabasic lithologies respectively. This model for calculating r_0, *E* and D_0 (equations 2, 3 and 5) should be thought of as an updated version of the model presented by van Westrenen et al. (2007), which incorporates additional experimental data published over the last eight years.

In addition to the above phases partition coefficients for ferropericlase, stishovite, olivine, magnesite and clinopyroxene were used throughout modelling. For ferropericlase a new lattice strain fit to data from Walter et al. (2004) was produced. Data for clinopyroxene in peridotitic assemblages and magnesite were taken from Dasgupta et al. (2009 experiment M318) and eclogitic clinopyroxene data were used from Suzuki et al. (2012 experiment U238). Values for olivine were taken from the compilation presented by Dasgupta et al. (2009). The partition coefficients for all elements in stishovite were assumed to be 0.001 as we are unaware of any reported values for trace element partitioning into this phase, which was assumed to be negligible. All partition coefficients used throughout this paper are summarised in table 1.

3. RESULTS

3.1 Juina-5 inclusions' trace element compositions

The results of trace element analyses of Juina-5 inclusions are presented in table 2, with data for inclusions interpreted as former bridgmanite, calcium silicate perovskite, NAL and CF phases, and majoritic garnet. The data are plotted as bulk silicate earth normalised (McDonough, 2001) spider diagrams (figure 4) and rare earth element diagrams (figure 5). Diamond and inclusion sample names used in this paper match those used in Thomson et al. (2014). Where individual inclusions have been analysed multiple times, all individual analyses are reported in table 1 and plotted in figures 4 and 5. It is observed that repeated analyses of the same inclusion sometimes produce differing abundances. As an example, the CF phase inclusion Ju5-20 was analysed in the same location twice, producing notably different results. This heterogeneity is caused by the composite mineralogy of the Juina-5 inclusions. We acknowledge that there are, therefore, uncertainties associated with the inclusions compositions. However, in most cases repeated analyses give similar results, and the reported analyses vastly enhance a very limited global dataset. The Juina-5 majorite and 'calcium perovskite' inclusions, which are particularly important in the modelling performed here, are either homogeneous or have heterogeneity on a very short length-scale that is averaged out in the reported analyses.

Five composite inclusions of former 'bridgmanite' were analysed and generally observed to be enriched in high field strength elements (HFSE) Nb, Ta, Zr and Hf relative to the bulk silicate Earth (BSE). They appear to have a strong depletion in Sr, as this element regularly falls below detection limits. They are depleted in light-mid REE, with the concentration of most of these elements in the majority of analyses falling below detection limits. The concentration of heavy rare earth elements (HREE) is approximately the same as BSE. This suggests their REE contents have a positively sloping pattern from La to Lu, a feature that reflects experimentally determined mineral/melt partition coefficients of bridgmanite (Corgne et al., 2005; Hirose et al., 2004; Walter et al., 2004). This agreement between analysed trace element pattern shape and experimental partition coefficients supports the previous interpretations that these inclusions are former bridgmanite (Thomson et al., 2014; Walter et al., 2011). Interesting features of the former 'bridgmanite' trace element patterns are the significant negative Ce anomaly ($Ce^* < 0.015$) and low Y/Ho ratio observed in several inclusions.

The four analysed former 'calcium silicate perovskite' inclusions, like those analysed in previous studies (Bulanova et al., 2010; Walter et al., 2008), are extremely enriched in all trace elements except for the large ion lithophile elements (LILE; Rb, Ba and Li). REE concentrations range from

between ~ 70 and 25,000 times BSE and have a negative slope from LREE to HREE. The HFSE are also highly enriched compared with BSE, but are relatively depleted compared with the REE abundances. Uranium and thorium concentrations reach up to ~55,000 times BSE (Ju5-115c), but are only 30 times BSE in other inclusions (Ju5-52b). The least enriched inclusion (Ju5-52b) is a titanium-free, walstromite structured, $CaSiO_3$ mineral whereas the remaining are composite $CaSiO_3$ – $CaTiO_3$ inclusions (Thomson et al., 2014). The enriched trace element characteristics of these inclusions are very similar to those described by Walter et al. (2008). It is observed that three of the inclusions possess a positive Ce anomaly (Ce* 1.2 - 1.8), whilst Ju5-82 also has a small negative Eu anomaly (Eu* ~ 0.7).

The trace element compositions of two majorite garnet inclusions are also similar to those observed in previous studies (e.g. Moore et al., 1991; Tappert et al., 2005). They are depleted in LREE (~ 0.1 times BSE) with normalised abundances increasing towards the HREE, which are significantly enriched when compared to the BSE (~ 100 times higher than BSE). They also show strong enrichment in Zr and Hf. Both analysed inclusions have a distinct negative Eu anomaly (Eu* = 0.52 & 0.57).

The trace element compositions of eight former 'NAL' and/or 'CF phase' minerals have been measured. These data provide the first insights into the possible abundances of trace elements in these minerals since there is currently no experimental data available for trace element partitioning into these phases. Analyses reveal that the LILE are likely compatible in these high-pressure alkaline minerals, with Ba depleted relative to Rb and Li. Several of the inclusions contain high concentrations (above BSE) of Th, U, Nb and Ta. The concentrations of the remaining elements in most samples were below detection limits, and where measured are similar to or slightly below the concentrations of BSE, with a notable depletion in Y relative to Dy and Ho. There is a strong negative Ce anomaly present in the normalised REE patterns of several of these inclusions (largest is Ce* ~ 0.065) and also a tentative suggestion that the data reveals a positive trend moving from LREE to HREE.

4. Discussion

The main aim of this work is to examine whether the trace element composition of silicate inclusions in superdeep diamonds are compatible with the hypothesis that they formed during the interaction of low-degree carbonated slab melts and ambient peridotite. To this end, simple models have been generated to calculate the expected composition of ambient mantle phases, the potential source rock compositions of individual inclusions and the sequence of mineral compositions created during

fractional crystallisation of an enriched melt. Throughout the following discussion, specific features of Juina-5 and global superdeep inclusions in combination with the results of these models are examined.

4.1 Is inclusion enrichment an indicator of a low-degree melt source?

In order to compare the trace element composition of the inclusions with ambient mantle lithologies a simple model that calculates the expected compositions of subsolidus phase assemblages is used. This approach combines the mineral/melt partition coefficients for coexisting minerals with the assumptions that trace element mass balance is achieved and the total trace element budget of the assemblage is fixed. It was assumed that peridotite and MORB have bulk trace element compositions (X_i^{total}) of the bulk silicate Earth (McDonough, 2001) and ALL-MORB (Gale et al., 2013) respectively. Under these assumptions the following mass balance can be written:

$$X_i^{total} = \alpha X_i^A + \beta X_i^B + \gamma X_i^C \qquad \text{(eq. 6)}$$

$$X_i^A = X_i^{total} \Big/ \left(\alpha + \beta \frac{D_i^{B/melt}}{D_i^{A/melt}} + \gamma \frac{D_i^{C/melt}}{D_i^{A/melt}} \right) \qquad \text{(eq. 7)}$$

Where X_i^A, X_i^B, X_i^C are the concentrations of trace element *i* in phase A, B, C. and α, β, γ are the proportions of phase A, B and C in the phase assemblage. Equation 7 can be re-written for X_i^B or X_i^C in a similar manner. Employing this approach, the expected trace element compositions of phases in subsolidus pyrolite and MORB phase assemblages at transition zone and uppermost lower mantle conditions were calculated. The predicted compositions of subdolidus garnet, calcium perovskite and bridgmanite minerals were extracted. For garnet and calcium silicate perovskite, calculations were performed for a transition zone assemblage at 1600° C consisting of olivine + garnet + calcium perovskite (in mass proportions of 60:30:10) and garnet + calcium perovskite + stishovite (80:10:10) for peridotite and MORB compositions, respectively. The composition of bridgmanite and calcium perovskite in subsolidus peridotite at 2300 °C was calculated for an assemblage consisting of bridgmanite + calcium perovskite + ferropericlase (80:10:10). A MORB-hosted bridgmanite composition cannot be calculated because there are no known partition coefficients for NAL or CF phase, both of which are significant components of a lower mantle metabasic assemblage. The calculated subsolidus mineral compositions is compared with the Juina-5 inclusions in figure 6.

The trace element enrichment observed in all Juina-5 'calcium silicate perovskite' inclusions is significantly higher than that expected in subsolidus assemblages. Similar high enrichments are also observed in 'calcium silicate perovskite' inclusions from Collier-4 in the Juina region (Bulanova et al.,

2010; Walter et al., 2008). Even if calcium perovskite were only 0.1 wt.% of a subsolidus assemblage (instead of 10 wt.%) this only increases expected trace element abundances by ~ one order of magnitude, which still does not explain the elevated abundances of many Juina-5 (this study) and Collier-4 (Bulanova et al., 2010) inclusions. Subsolidus minerals are also not expected to possess the significant negative relative anomalies in Sr, Hf and Zr that are observed in the diamond-hosted inclusions. Modelled subsolidus phases have flat normalised REE patterns, which also contrast with the fractionated (sloping) patterns observed in many inclusions. Overall, we conclude that former 'calcium silicate perovskite' inclusions from Juina-5 and Collier-4 are not trapped fragments of ambient mantle material, consistent with the interpretation based on major elements (notably the high Ti and low Mg contents, e.g. Armstrong et al., 2012). Alternatively, high trace element enrichments are consistent with, and often characteristic of, crystallisation from a low-degree melt (Walter et al., 2008). Additionally, the strong depletions of Sr, as is demonstrated in section 4.3, could be the signature of dehydration of subducting rocks at shallow subarc conditions. Depletions in Zr and Hf suggest the presence of accessory zircon or baddeleyite in the source region of 'calcium perovskite' inclusions, also an indicator of crustal material. The composition of some global inclusions (Hutchison, 1997; Kaminsky et al., 2001; Stachel et al., 2000b) do overlap the abundances expected in subsolidus mantle assemblages. However, despite their low enrichments, many of these inclusions also possess depletions of Sr, Hf and Zr and have sloping REE patterns. It is suggested that they were also created from crustal/slab melts. Former 'calcium perovskite' inclusions observed from Machado River (Burnham et al., *this issue*) are significantly more depleted than those from all other localities, possessing trace element abundances below amounts expected in subsolidus mantle assemblages. Possible explanations for varying enrichment of former 'calcium perovskite' inclusions are discussed below.

Majoritic garnet inclusions from Juina-5, and other worldwide diamonds, are all more enriched than calculated garnet in subsolidus assemblages. The Juina-5 inclusions themselves are some of the least enriched diamond-hosted majoritic garnets in the global dataset. In contrast with the calculated composition of subsolidus calcium perovskite the quantity of trace elements in garnet is virtually insensitive to its abundance in the mantle, provided majorite is in equilibrium with calcium perovskite. Thus, it is assumed that the elevated enrichment of worldwide garnet inclusions is the signature that they formed in equilibrium with melt. Many garnet inclusions also have a clear negative Sr anomaly, whereas subsolidus majorite should have a positive anomaly. This is unambiguous evidence that superdeep majoritic garnet inclusions formed in equilibrium with a low-degree melt of subducted material that acts to concentrate incompatible elements.

Two crucial consequences of the interpretation that Juina region 'calcium perovskite' and global majoritic garnet inclusions formed from slab melts are that in order to produce a suitably enriched melt, i) the residual phase assemblage must not contain any phases that significantly sequester incompatible elements and ii) the degree of melting must be very small. These two constraints virtually exclude the possibility that calcium silicate perovskite is saturated in the melting phase assemblage, because this would retain almost all trace elements in the residue remaining after melting. Highly enriched low-degree melts, therefore, can probably only be produced prior to the saturation of calcium perovskite in subducting slab assemblages, i.e. at pressures less than 17-20 GPa (e.g. Kiseeva et al., 2013a; Zhang and Herzberg, 1994). This is consistent with the production of diamond forming melts of oceanic crust in the transition zone as the carbonated MORB solidus intersects slab geotherms between ~ 350 and 600 km depth (Thomson et al., 2016). This depth range is consistent with barometry estimates for the formation pressures of diamond-hosted garnet inclusions (Beyer, 2015; Collerson et al., 2010; Harte, 2010; Stachel, 2001). Although, it is unclear whether majorite barometers can be applied to natural inclusions, given they are believed to have co-crystallised from a melt with calcium perovskite (Thomson et al., 2016) and undergone some re-equilibration during uplift (Harte and Cayzer, 2007; Thomson et al., 2014) that may not have been fully accounted for in reported compositions. Furthermore, the enriched 'calcium perovskite' inclusions also all have an extremely low MgO content, which precludes their formation in equilibrium with bridgmanite (Armstrong et al., 2012; Walter et al., 2008), a feature that is also consistent with the formation of these diamonds in the transition zone at depths less than 600 km. One potential explanation for the formation of the less enriched 'calcium perovskite' inclusions (Hutchison, 1997; Kaminsky et al., 2001; Stachel et al., 2000b; Burnham et al., *this issue*) could be that they crystallised from slab melts at higher pressures. Beyond ~ 600 km depth, where calcium perovskite is stable in subducting assemblages, slab melts would be significantly less enriched in trace elements, and thus so would any inclusions produced by crystallisation of these melts. Inclusions from Kankan and São Luis (Hutchison, 1997; Kaminsky et al., 2001; Stachel et al., 2000b) also have low MgO contents, suggesting they crystallised in the very deepest portions of the upper mantle, not in equilibrium with bridgmanite. The even more depleted 'calcium perovskite' inclusions in Machado River diamonds have a higher MgO content (a few weight percent), which is likely to be an indicator they crystallised in equilibrium with bridgmanite (Burnham et al., *this issue*). This suggests that 'calcium perovskite' inclusions sample a range of formation depths.

Juina-5 'bridgmanite' inclusions are also somewhat enriched compared with modelled subsolidus bridgmanite, especially for LREE-MREE and HFSEs (figure 6c). Measured levels of HREE elements in

these inclusions are similar to the concentrations expected in ambient lower mantle bridgmanite. The interrupted nature of the data, due to analyses for several elements falling below detection limits makes it unclear whether the 'bridgmanite' inclusions are significantly enriched compared with the compositions expected in ambient mantle assemblages or not. Additionally, it should be noted that the subsolidus lower mantle bridgmanite composition was calculated using partition coefficients appropriate for 2300 °C, ~ 500-600 °C hotter than the expected adiabatic temperature at the top of the lower mantle (Katsura et al., 2010). Section 2.2 demonstrates the large influence that temperature has on trace element partitioning in the case of garnet. However, because the effects of temperature on partitioning vary between different minerals, it is not possible to estimate whether lower temperature assemblages should contain more or less enriched bridgmanite than in the current model. Therefore, due to these two sources of uncertainty, it cannot be concluded whether or not 'bridgmanite' inclusions are enriched compared with ambient mantle phases. A negative Sr anomaly is identified in some of the 'bridgmanite' inclusions, which serves as evidence they were likely crystallised from slab melts.

Figure 6d compares the composition of natural intraplate carbonatite melts (Hoernle et al., 2002) with the calculated melts in equilibrium with Juina-5 'calcium silicate perovskite' and garnet inclusions. Calculated and natural melts have similar REE slopes and trace element concentrations, demonstrating that melts of necessarily enriched compositions are plausible for diamond formation. The disagreement between Zr and Hf in the calculated and natural melts could be explained either by the effect of pressure on their partition coefficients, or the presence of baddeleyite/zircon in the residual assemblage that produced the natural carbonatite melts. It also confirms the suitability of carbonatite melts for explaining the compositions of diamond-hosted inclusions. It has been suggested that the isotopic signatures of intraplate carbonatite lavas require input from recycled ocean floor material (Doucelance et al., 2014). Given the similarities between the melt compositions necessary for inclusion crystallisation and these erupted carbonate liquids it is possible that both share a common origin from melting of recycled material in the transition zone.

4.2 Eu, Ce and Y/Ho anomalies

Common to many of the Juina-5 inclusions are Ce, Eu and Y anomalies. Negative Eu anomalies, similar to those observed in the Juina-5 majoritic garnet inclusions (figure 5c, Eu* = 0.52 & 0.57 for Ju5-32 & Ju5-83 respectively), are generally accepted to result from the fractionation of feldspar (Philpotts and Schnetzler, 1968). However, because feldspar is only stable at crustal pressures, similar observations in superdeep diamonds have previously been interpreted as evidence for the involvement of

subducted crust in the formation of the diamond-hosted inclusions (Harte et al., 1999; Stachel et al., 2000a; Tappert et al., 2005). This interpretation is certainly consistent with the recycled isotopic signatures in superdeep diamonds (Burnham et al., 2015b; Ickert et al., 2015).

Negative Ce anomalies are also often associated with subducted material, as they are widely observed in pelagic sediments containing high levels of organic debris (Hole et al., 1984; Toyoda et al., 1990). It is conceivable, therefore, that the incorporation of the large negative Ce anomalies observed in Ju5-43 'bridgmanite' and several NAL phase inclusions are created by the direct incorporation of recycled material. However, three of the four analysed 'calcium silicate perovskite' inclusions possess a positive Ce anomaly, as do some of the 'calcium perovskite' inclusions reported by Bulanova et al. (2010). It seems unlikely that anomalies of opposite sense could be incorporated into inclusions of a single diamond suite if they are truly formed simply by inheriting any signatures that pre-exist in their slab-derived source material. It is also unlikely that subducted sedimentary material could be responsible for the observed anomalies, because this requires the sedimentary package to survive subduction unaltered to depths greater than 400 km despite the expected occurrence of slab dehydration in the sub-arc environment and possible high slab surface temperatures. Further, it is unclear whether organic material could even generate a Ce anomaly of the same size observed in Ju5-43, approximately 2 orders of magnitude; pure nano-fossil ooze has been observed to have a negative Ce anomaly of slightly less than one order of magnitude (Hole et al., 1984). It is perhaps more plausible that the Ce anomalies are generated because the melts responsible for diamond and inclusion growth contain a mixture of Ce^{3+} and Ce^{4+}. In this scenario it is possible that Ce^{4+} fractionates into coexisting phases during the melting and inclusion formation processes. It has been observed that some natural baddeleyite minerals contain a significant positive Ce anomaly (Schärer et al., 2011), as Ce^{4+} is approximately 100 times more compatible in ZrO_2 than Ce^{3+} (Klemme et al., 2003). Similar observations of Ce anomalies have been made in other Zr-rich minerals, e.g. zircon (Schärer et al., 2011) and wadeite (Jaques, 2016). Given that an exsolved phase of baddeleyite was observed in two of the 'calcium perovskite' inclusions (Thomson et al., 2014) and depletions of Zr and Hf in trace element patterns, saturation of a Zr-rich accessory phase in the diamond formation process is a reasonable possibility. If Ce anomalies in diamond-hosted inclusions do indeed result from the presence of both Ce valence states in deep melts, the magnitude of anomalies must contain information about the oxygen fugacity during diamond growth. Although the experimental data to allow extraction of this information doesn't yet exist it is possible to comment that whilst Ce^{4+} is generally extremely low in natural melt compositions it is enhanced at high fO_2, in alkaline melts, at low temperatures and possibly with increasing pressures (Burnham and Berry,

2014). Therefore it is possible that near solidus MORB melts, which are alkaline carbonatites generated at relatively low temperatures (Thomson et al., 2016), promote the occurrence of large Ce anomalies because they naturally contain high levels of Ce^{4+}.

It is possible that the observed Eu anomalies could be created in a similar manner, from mixed Eu^{2+} and Eu^{3+} in melts, and have no relation to crustal feldspar. By assuming that Sr^{2+} and Eu^{2+} are geochemical twins the largest feasible Eu anomaly that can be created in majoritic garnet resulting only from mixed Eu valence states in the melt, i.e. with no crustal plagioclase signature, can be estimated. Using partition coefficients for peridotitic and metabasic majorite in table 1, D^{Eu2+} is approximately 10-30 times smaller than D^{Eu3+}, which implies Eu* of approximately 0.03 – 0.1 are possible from a melt with $Eu^{2+}/Eu^{tot} = 1$. Thus, it is possible that europium anomalies could be generated during carbonated melting in the transition zone. However, current data on Eu oxidation state in melts suggests it is unlikely that both Eu^{2+} and Ce^{4+} would coexist (Burnham et al., 2015a), but the speciation of Eu and Ce in high pressure carbon-bearing melts requires investigation before this possibility can be ignored.

Significant Y/Ho anomalies are also observed in Juina-5 'calcium silicate perovskite', 'bridgmanite' and 'NAL/CF phase' inclusions. Unlike Ce and Eu, Y can only exist as Y^{3+}. Therefore, these anomalies cannot be explained by fractionation due to the presence of multiple valence states of Y. Similar negative Y/Ho anomalies have been observed in seafloor ferromanganese nodules and seawater samples collected from above the East Pacific Rise (Ohta et al., 1999). These anomalies are associated with the complexation of yttrium in hydrous fluids/melts (Bau, 1999; 1996). Negative Y/Ho anomalies are also been observed in natural carbonatite lavas from intraplate volcanoes, such as the Cape Verde and Canary Islands (Hoernle et al., 2002, figure 6d), although these have not been explained. Whatever the exact explanation, these anomalies must be the result of low temperature fractionation to allow the subtleties of coordination environment to be significant. Therefore, we suggest that Y/Ho anomalies are another signature of the involvement of subducted material in the growth of superdeep diamonds.

4.3 Source rock of melts

The above discussion concludes that the Juina-5 inclusions contain many indicators that they crystallised under upper mantle conditions from a low-degree melt. From the trace element characteristics themselves, the presence of Sr, Zr and Hf anomalies suggest that this melt is linked to subducted crust foundered in the transition zone. To further examine whether 'calcium perovskite'

inclusions are indeed compatible with crystallisation in the transition zone (Thomson et al., 2016) we attempt to determine source rock compositions that could have generated the inclusions (figure 7). The source rock composition (green line) is calculated assuming that the melt in equilibrium (red line) with individual inclusions (blue line) is produced during a non-modal fractional melting process. A re-arrangement of the equation for accumulated non-modal fractional melts is used to calculate the trace element composition of the source lithology:

$$C^0 = \frac{\bar{c}^l F}{\left[1-\left(1-{}^{PF}/_{D_o}\right)^{1/P}\right]} \qquad \text{(eq. 8)}$$

Assuming that the degree of melting (F) is 1 %, D_0 is calculated for a phase assemblage consisting 64 % garnet, 15 % clinopyroxene, 15 % stishovite and 5 % carbonate as observed for a subsolidus carbonated eclogite at 13 GPa (Thomson et al., 2016). P is calculated from the melting reaction observed at 13 GPa (Thomson et al., 2016):

$$0.54\ clinopyroxene + 0.67\ magnesite = 1\ melt + 0.15\ garnet + 0.09\ stishovite \qquad \text{(eq. 9)}$$

This calculation was performed in a Monte Carlo simulation with 10,000 cycles, where errors where varied randomly in each cycle assuming a Gaussian distribution within 1σ = 10 % of the measured value. The dashed lines in figure 7 are 95 % confidence intervals in the calculated melt composition and define the range of calculated source rock compositions. Calculated source rock compositions can be compared with the that of the average oceanic crust, ALL-MORB (Gale et al., 2013). However, because it is expected that the subducting slab will have experienced dehydration in the sub-arc environment prior to this melting process the source rock composition is compared with a "processed MORB". The composition of "processed MORB" is calculated by assuming 7.5 % dehydration occurs at each of 2.5, 4 and 6 GPa using partition coefficients for MORB/hydrous fluid partitioning (Kessel et al., 2005; Klimm et al., 2008). The "processed MORB" composition only illustrates the potential effects that slab dehydration may have on slab chemistry, it is not believed to capture the full complexity of MORB dehydration processes.

The model employed is simplistic, and serves only to illustrate whether or not the hypothesis that inclusions are generated from slab-derived carbonatites is generally consistent with their trace element chemistries. The model ignores the potential effects of accessory phases and makes the assumption that melting is isobaric, occurring at ~ 15 GPa, and can be described by the melting reactions observed in Thomson et al. (2016). It also assumes that partition coefficients for all phases in modelling are well known at the pressure and temperature conditions appropriate for this reaction. Unfortunately, as summarised in section 2.2 this is not the case, because there is

insufficient experimental data to account for the effects of P, T and composition on partition coefficients. Therefore, this model can only currently indicate whether the hypothesis of diamond formation by slab melt crystallisation is feasible, or is completely inconsistent with the trace element composition of natural inclusions.

With these limitations in mind, the results of modelling for Ju5-115c and Ju5-82 demonstrate they could form from a source rock containing features expected in a subducted MORB lithology. Both models predict a source rock that contains a significant negative Sr anomaly, a feature created during slab dehydration in the shallow subarc environment. Calculated source rock compositions have relatively flat BSE normalised REE abundances, a common feature in both ALL-MORB and "processed MORB". Modelled source rock compositions also generally have trace element abundances that overlap, or are in the range of, those of subducted crustal rocks. If the temperature of melting was lower than 1600 °C the calculated equilibrium melt and source rock compositions would be less enriched, due to the effect of temperature on partition coefficients. Thus lower temperatures, as would are consistent with the conditions for slab melting (Thomson et al., 2016) might reduce the enrichment of the Ju5-115c source rock to match the slab lithologies, however the magnitude of this effect cannot be estimated. Thus, it appears from this modelling that the compositions of Juina-5 'calcium perovskite' inclusions, at least in general, are consistent with an origin from crystallising slab melts at transition zone depths.

4.4. Inclusions as a record of fractional crystallisation sequence

Walter et al. (2008) suggested that the trace element chemistry of all measured Collier-4 inclusions could be related to each other if they result from fractional crystallisation of a common parent melt that has undergone varying degrees of evolution, in other words, if they record a liquid line of descent as a low-degree slab melt crystallises. If all diamond-hosted inclusions are formed by a common petrological process it is possible that all superdeep inclusions from similar depth intervals, independent of their geographical location, may be related in a similar way. Figure 8a demonstrates that there is a strong correlation between the REE chemistry of majoritic garnet inclusions and their major element chemistry, that is not a function of crystallisation pressure. Sm/Lu is used in figure 8a as a proxy for the slope of the garnet REE patterns, and is plotted against Ca content (calculated per formula unit assuming 12 oxygens). This correlation could be interpreted as a record of a melt crystallisation process, however, it could also theoretically be produced by the variation of partition coefficients with inclusion composition. To ensure that this correlation is not only the result of the latter possibility, the composition of the melt in equilibrium with each individual inclusion was

calculated (figure 8b) using a majorite barometer (Beyer, 2015) to estimate the inclusion formation pressures. As the calculated melt compositions also vary significantly in composition the correlation between Ca and Sm/Lu must reflect the variation of melt compositions that inclusions crystallise from. The systematic evolution in the calculated melts towards flatter REE patterns (and lower REE abundances) with decreasing Ca content of the inclusions (figure 8a) suggests that they may indeed record the evolution of fractionating melts. It also implies that the primary diamond-forming melt in the transition zone would be calcium-rich, an observation that is consistent with the composition of subducted MORB-derived carbonatites (Hammouda, 2003; Thomson et al., 2016).

We have further investigated the possibility that several diamond-hosted inclusions are associated with one another by running a simple fractional crystallisation model (figure 9). Starting from the trace element composition of the melt in equilibrium with the most highly enriched Juina-5 'calicum silicate perovskite' inclusion, a forward model was run where small quantities of calcium perovskite and majoritic garnet in equilibrium with the melt composition were sequentially removed to simulate fractional crystallisation. During each cycle the compositions of the crystallising phases and evolving melt were recorded. The mass of material (in arbitrary units) removed and the relative proportions of garnet and calcium perovskite that crystallise during each model step were varied. Initially partition coefficients calculated for the composition of the garnet Ju5-32 at 17.65 GPa (pressure calculated using barometer presented by Beyer, 2015) and 1600 °C were used. Subsequently the effects of changing pressure and temperature on the composition of the fractionating majoritic garnet was investigated by using partition coefficients appropriate to each scenario (figure 9b). Since the partition coefficients for calcium silicate perovskite are significantly larger than those for majoritic garnet, changing the relative proportions of crystallising phases only has a small influence on model results. The results of two models with the composition of diamond-hosted inclusions are compared in figure 9, one where majoritic garnet and calcium perovskite crystallise in a 10:1 ratio (figure 9a) and a second where only calcium perovskite crystallisation is considered (figure 9b).

It is observed that the REE patterns of all Juina-5 'calcium silicate perovskite' and majoritic garnet inclusions are reproduced fairly well by our fractional crystallisation model. Furthermore, the majority of the trace element compositional spectrum observed in global majorite compositions is also reproduced by changes in the pressure/temperature conditions of garnet crystallisation. This confirms that all superdeep diamonds could indeed be generated by a common petrogenetic process; the crystallisation of low-degree slab melts. If diamonds do represent the products of slab melting, it could imply that diamonds from each locality sample slab melts from a common depth interval. This

can be understood by linking all the diamonds from Juina-5 to a single slab geotherm, which would be expected to intersect the slab's carbonated solidus across a narrow pressure interval. Thus, even if diamonds were produced in multiple episodes they could be expected to generate similar inclusions.

5. CONCLUSIONS

The trace element compositions of 'calcium perovskite', majoritic garnet, 'bridgmanite' and 'NAL/CF phase' inclusions in superdeep diamonds from Juina-5 have been presented and examined. The inclusions are highly enriched in trace elements, to the extent that they are highly unlikely to represent trapped fragments of pristine ambient mantle. Instead, they are far more likely to have crystallised from a low-degree melt. Negative anomalies of Sr, Hf and Zr observed in inclusions point to an origin from crustal material that has undergone dehydration during subduction. In order to explain the high enrichment of Juina-5, Collier-4 'calcium perovskite' and global majoritic garnet inclusions, diamond-forming melts must be produced from an assemblage that does not contain calcium perovskite in the residue. Thus some superdeep diamonds previously believed to have been exhumed from the lower mantle, were in fact formed at depths shallower than 600 km. Several inclusions possess Ce, Eu and Y/Ho anomalies; all features that have often been associated with crustal processes. However, at least in the case of the inclusion Ce anomalies, it is unlikely that they were created by the inheritance of signatures present in the subducted crust due to their association with sedimentary material and their large magnitude. Instead, they probably reveal the presence of mixed Ce species in melts present during diamond formation. Ultimately this information might be used to constrain the oxygen fugacity of diamond growth in the Juina-5 source region.

Overall, the trace element compositions of Juina-5 and global inclusions are consistent with the hypothesis that they crystallised from low-degree slab melts. It also appears that diamond-hosted inclusions from a single locality might record the fractional crystallisation sequence melts throughout interaction of slab melts with the ambient mantle, and global majoritic garnet compositions record evidence for the variation in subducting slab geotherms. This provides further evidence that superdeep diamonds sample a continuous spectrum of inclusion compositions that are related to the interaction of crustal and mantle materials, and therefore diamonds should no longer be categorised by a scheme that only associates them with end-members of this continuum. Superdeep diamonds from other global localities have lower enrichment of trace elements, which could be an indicator of diamond growth beyond 600 km depth. Coupled with major element chemistries, this highlights that inclusion trace element enrichments should be used as a primary indicator for identifying diamonds that have been exhumed from the deepest portions of the upper mantle or beyond.

ACKNOWLEDGEMENTS

We thank Richard Hinton and John Craven from the EIMF for their contribution to this work. We acknowledge support from the Natural Environmental Research Council, grant NE/J500033/1 awarded to ART and NE/J008583/1 awarded to MJW and SCK. We also acknowledge the EIMF award IMF438/0511. Finally, we thank the reviewers, Ben Harte and an anonymous reviewer, and the editor, Steven Shirey for constructive comments.

citations from figure and table captions (Corgne et al., 2005; Corgne and Wood, 2002; Dalou et al., 2009; Hirose et al., 2004; Taura et al., 2001; Walter et al., 2004) (Adam and Green, 2001; Bulanova et al., 2010; Davies et al., 2004b; Hutchison, 1997; Kaminsky et al., 2001; Kelemen et al., 2003; Moore et al., 1991; Stachel et al., 2000a; Sweeney et al., 1995; Tappert et al., 2005)

REFERENCES

Adam, J., Green, T., 2001. Experimentally determined partition coefficients for minor and trace elements in peridotite minerals and carbonatitic melt, and their relevance to natural carbonatites. Eur.J.Mineral. 13, 815–827. doi:10.1127/0935-1221/2001/0013/0815

Armstrong, L.S., Walter, M.J., Tuff, J.R., Lord, O.T., Lennie, A.R., Kleppe, A.K., Clark, S.M., 2012. Perovskite phase relations in the system CaO-MgO-TiO_2-SiO_2 and implications for deep mantle lithologies. Journal of Petrology 53, 611–635. doi:10.1093/petrology/egr073

Bau, M., 1999. Scavenging of dissolved yttrium and rare earths by precipitating iron oxyhydroxide: experimental evidence for Ce oxidation, Y-Ho fractionation, and lanthanide tetrad effect. Geochimica et Cosmochimica Acta 63, 67–77. doi:10.1016/S0016-7037(99)00014-9

Bau, M., 1996. Controls on the fractionation of isovalent trace elements in magmatic and aqueous systems: evidence from Y/Ho, Zr/Hf, and lanthanide tetrad effect. Contr. Mineral. and Petrol. 123, 323–333. doi:10.1007/s004100050159

Bennett, S.L., Blundy, J., Elliott, T., 2004. The effect of sodium and titanium on crystal-melt partitioning of trace elements. Geochimica et Cosmochimica Acta 68, 2335–2347. doi:10.1016/j.gca.2003.11.006

Beyer, C., 2015. Geobarometry, phase relations and elasticity of eclogite under conditions of Earth's upper mantle. Bayreuth.

Bindi, L., Dymshits, A.M., Bobrov, A.V., Litasov, K.D., Shatskiy, A.F., Ohtani, E., Litvin, Y.A., 2011. Crystal chemistry of sodium in the Earth's interior: The structure of $Na_2MgSi_5O_{12}$ synthesized at 17.5 GPa and 1700 °C. American Mineralogist 96, 447–450. doi:10.2138/am.2011.3716

Blundy, J., Wood, B., 1994. Prediction of crystal-melt partition coefficients from elastic moduli. Nature 372, 452–454. doi:10.1038/372452a0

Blundy, J.D., Falloon, T.J., Wood, B.J., Dalton, J.A., 1995. Sodium partitioning between clinopyroxene and silicate melts. J. Geophys. Res. 100, 15501–15515. doi:10.1029/95JB00954

Bobrov, A.V., Litvin, Y.A., Kuzyura, A.V., Dymshits, A.M., 2014. Partitioning of trace elements between Na-bearing majoritic garnet and melt at 8.5 GPa and 1500–1900 °C. Lithos 189, 159–166. doi:10.1016/j.lithos.2013.11.003

Brenker, F., Brenker, F.E., Vincze, L., Vekemans, B., Vincze, L., Vekemans, B., Nasdala, L., Stachel, T., Vollmer, C., Kersten, M., Somogyi, A., Adams, F., Joswig, W., 2005. Detection of a Ca-rich lithology in the Earth's deep (>300 km) convecting mantle. EPSL 236, 579–587. doi:10.1016/j.epsl.2005.05.021

Brey, G.P., Bulatov, V., Girnis, A., Harris, J.W., Stachel, T., 2004. Ferropericlase—a lower mantle phase in the upper mantle. Lithos 77, 655–663. doi:10.1016/j.lithos.2004.03.013

Bulanova, G.P., Walter, M.J., Smith, C.B., Kohn, S.C., Armstrong, L.S., Blundy, J., Gobbo, L., 2010. Mineral inclusions in sublithospheric diamonds from Collier 4 kimberlite pipe, Juina, Brazil: subducted protoliths, carbonated melts and primary kimberlite magmatism. Contr. Mineral. and Petrol. 160, 489–510. doi:10.1007/s00410-010-0490-6

Burnham, A.D., Berry, A.J., 2014. The effect of oxygen fugacity, melt composition, temperature and pressure on the oxidation state of cerium in silicate melts. Chemical Geology 366, 52–60. doi:10.1016/j.chemgeo.2013.12.015

Burnham, A.D., Berry, A.J., Halse, H.R., Schofield, P.F., Cibin, G., Mosselmans, J.F.W., 2015a. The oxidation state of europium in silicate melts as a function of oxygen fugacity, composition and temperature. Chemical Geology 411, 248–259. doi:10.1016/j.chemgeo.2015.07.002

Burnham, A.D., Thomson, A.R., Bulanova, G.P., Kohn, S.C., Smith, C.B., Walter, M.J., 2015b. Stable isotope evidence for crustal recycling as recorded by superdeep diamonds. Earth and Planetary Science Letters 432, 374–380.

doi:10.1016/j.epsl.2015.10.023
Burnham, A.D., Bulanova, G.P., Smith, C.B., Whitehead, S.C., Kohn, S.C., Gobbo, L., Walter, M.J., 2016. Diamonds from the Machado River alluvial deposit, Rondônia, Brazil, derived from both lithospheric and sublithospheric mantle. Lithos *this issue*, doi:10.1016/j.lithos.2016.05.022
Chang, S.J., Ferreira, A.M.G., Ritsema, J., van Heijst, H.J., Woodhouse, J.H., 2015. Joint inversion for global isotropic and radially anisotropic mantle structure including crustal thickness perturbations. Journal of Geophysical Research B: Solid Earth 120, 4278–4300. doi:10.1002/2014JB011824
Collerson, K.D., Collerson, K.D., Williams, Q., Kamber, B.S., Kamber, B.S., Omori, S., Arai, H., Ohtani, E., 2010. Majoritic garnet: A new approach to pressure estimation of shock events in meteorites and the encapsulation of sub-lithospheric inclusions in diamond. Geochimica et Cosmochimica Acta 74, 5939–5957. doi:10.1016/j.gca.2010.07.005
Corgne, A., Armstrong, L.S., Keshav, S., Fei, Y., McDonough, W.F., Minarik, W.G., Moreno, K., 2012. Trace element partitioning between majoritic garnet and silicate melt at 10–17GPa: Implications for deep mantle processes. Lithos 148, 128–141. doi:10.1016/j.lithos.2012.06.013
Corgne, A., Liebske, C., Wood, B.J., Rubie, D.C., Frost, D.J., 2005. Silicate perovskite-melt partitioning of trace elements and geochemical signature of a deep perovskitic reservoir. Geochimica et Cosmochimica Acta 69, 485–496. doi:10.1016/j.gca.2004.06.041
Corgne, A., Wood, B.J., 2005. Trace element partitioning and substitution mechanisms in calcium perovskites. Contr. Mineral. and Petrol. 149, 85–97. doi:10.1007/s00410-004-0638-3
Corgne, A., Wood, B.J., 2002. CaSiO 3and CaTiO 3perovskite-melt partitioning of trace elements: Implications for gross mantle differentiation. Geophys. Res. Lett. 29, 1933. doi:10.1029/2001GL014398
Dalou, C., Koga, K.T., Hammouda, T., Poitrasson, F., 2009. Trace element partitioning between carbonatitic melts and mantle transition zone minerals: Implications for the source of carbonatites. Geochimica et Cosmochimica Acta 73, 239–255. doi:10.1016/j.gca.2008.09.020
Dasgupta, R., Hirschmann, M.M., McDonough, W.F., Spiegelman, M., Withers, A.C., 2009. Trace element partitioning between garnet lherzolite and carbonatite at 6.6 and 8.6 GPa with applications to the geochemistry of the mantle and of mantle-derived melts. Chemical Geology 262, 57–77. doi:10.1016/j.chemgeo.2009.02.004
Davies, R.M., Davies, R.M., Griffin, W.L., Griffin, W.L., O'Reilly, S.Y., O'Reilly, S.Y., Doyle, B.J., Doyle, B.J., 2004a. Mineral inclusions and geochemical characteristics of microdiamonds from the DO27, A154, A21, A418, DO18, DD17 and Ranch Lake kimberlites at Lac de Gras, Slave Craton, Canada. Lithos 77, 39–55. doi:10.1016/j.lithos.2004.04.016
Davies, R.M., Davies, R.M., Griffin, W.L., Griffin, W.L., O'Reilly, S.Y., O'Reilly, S.Y., McCandless, T.E., McCandless, T.E., 2004b. Inclusions in diamonds from the K14 and K10 kimberlites, Buffalo Hills, Alberta, Canada: diamond growth in a plume? Lithos 77, 99–111. doi:10.1016/j.lithos.2004.04.008
Doucelance, R., Bellot, N., Boyet, M., Hammouda, T., Bosq, C., 2014. What coupled cerium and neodymium isotopes tell us about the deep source of oceanic carbonatites. Earth and Planetary Science Letters 407, 175–186. doi:10.1016/j.epsl.2014.09.042
Draper, D.S., duFrane, S.A., Shearer, C.K., Jr., Dwarzski, R.E., Agee, C.B., 2006. High-pressure phase equilibria and element partitioning experiments on Apollo 15 green C picritic glass: Implications for the role of garnet in the deep lunar interior. Geochimica et Cosmochimica Acta 70, 2400–2416. doi:10.1016/j.gca.2006.01.027
Draper, D.S., van Westrenen, W., 2007. Quantifying garnet-melt trace element partitioning using lattice-strain theory: assessment of statistically significant controls and a new predictive model. Contr. Mineral. and Petrol. 154, 731–746. doi:10.1007/s00410-007-0235-3
Dwarzski, R.E., Draper, D.S., Shearer, C.K., Agee, C.B., 2006. Experimental insights on crystal chemistry of high-Ti garnets from garnet-melt partitioning of rare-earth and high-field-strength elements. American Mineralogist 91, 1536–1546. doi:10.2138/am.2006.2100
Gale, A., Dalton, C.A., Langmuir, C.H., Su, Y., Schilling, J.-G., 2013. The mean composition of ocean ridge basalts. Geochem. Geophys. Geosyst. 14, 489–518. doi:10.1029/2012gc004334
Grassi, D., Schmidt, M.W., Günther, D., 2012. Element partitioning during carbonated pelite melting at 8, 13 and 22GPa and the sediment signature in the EM mantle components. Earth and Planetary Science Letters 327-328, 84–96. doi:10.1016/j.epsl.2012.01.023
Hammouda, T., 2003. High-pressure melting of carbonated eclogite and experimental constraints on carbon recycling and storage in the mantle. Earth and Planetary Science Letters 214, 357–368. doi:10.1016/S0012-821X(03)00361-3
Harte, B., 2010. Diamond formation in the deep mantle: the record of mineral inclusions and their distribution in relation to mantle dehydration zones. Mineralogical Magazine 74, 189–215. doi:10.1180/minmag.2010.074.2.189
Harte, B., Cayzer, N., 2007. Decompression and unmixing of crystals included in diamonds from the mantle transition zone. Phys Chem Minerals 34, 647–656. doi:10.1007/s00269-007-0178-2
Harte, B., Harris, J.W., Hutchison, M.T., Watt, G.R., Wilding, M.C., 1999. Lower mantle mineral associations in diamonds from São Luiz, Brazil. Field Observations and High Pressure Experimentation A tribute to Francis R. Joe Boyd The Geochemical Society, Houston 125–153.
Harte, B., Harte, B., Harris, J.W., 1994. Lower Mantle Mineral Associations Preserved in Diamonds. Mineralogical Magazine 58A, 384–385. doi:10.1180/minmag.1994.58A.1.201
Harte, B., Hudson, N.F.C., 2013. Mineral Associations in Diamonds from the Lowermost Upper Mantle and Uppermost

Lower Mantle, in: Proceedings of 10th International Kimberlite Conference. Springer India, New Delhi, pp. 235–253. doi:10.1007/978-81-322-1170-9_15

Harte, B., Richardson, S., 2012. Mineral inclusions in diamonds track the evolution of a Mesozoic subducted slab beneath West Gondwanaland. Gondwana Research 21, 236–245. doi:10.1016/j.gr.2011.07.001

Hauri, E.H., Wagner, T.P., Grove, T.L., 1994. Experimental and natural partitioning of Th, U, Pb and other trace elements between garnet, clinopyroxene and basaltic melts. Chemical Geology 117, 149–166. doi:10.1016/0009-2541(94)90126-0

Hayman, P.C., Kopylova, M.G., Kaminsky, F.V., 2005. Lower mantle diamonds from Rio Soriso (Juina area, Mato Grosso, Brazil). Contr. Mineral. and Petrol. 149, 430–445. doi:10.1007/s00410-005-0657-8

Hirose, K., Shimizu, N., van Westrenen, W., Fei, Y., 2004. Trace element partitioning in Earth's lower mantle and implications for geochemical consequences of partial melting at the core–mantle boundary. Physics of the Earth and Planetary Interiors 146, 249–260. doi:10.1016/j.pepi.2002.11.001

Hoernle, K., Tilton, G., Le Bas, M.J., Duggen, S., Garbe-Schönberg, D., 2002. Geochemistry of oceanic carbonatites compared with continental carbonatites: mantle recycling of oceanic crustal carbonate. Contr. Mineral. and Petrol. 142, 520–542. doi:10.1007/s004100100308

Hole, M.J., Saunders, A.D., Marriner, G.F., Tarney, J., 1984. Subduction of pelagic sediments: implications for the origin of Ce-anomalous basalts from the Mariana Islands. Journal of the Geological Society 141, 453–472. doi:10.1144/gsjgs.141.3.0453

Hutchison, M.T., 1997. Constitution of the deep transition zone and lower mantle shown by diamonds and their inclusions.

Ickert, R.B., T, S., R A, S., J W, H., 2015. Extreme ^{18}O-enrichment in majorite constrains a crustal origin of transition zone diamonds. Geochemical Perspectives Letters 65–74. doi:10.7185/geochemlet.1507

Jaques, A.L., 2016. Major and trace element variations in oxide and titanate minerals in the West Kimberley lamproites, Western Australia. Miner Petrol 1–39. doi:10.1007/s00710-015-0420-4

Kaminsky, F., 2012. Mineralogy of the lower mantle: A review of "super-deep" mineral inclusions in diamond. Earth-Science Reviews 110, 127–147. doi:10.1016/j.earscirev.2011.10.005

Kaminsky, F., Wirth, R., Wirth, R., Matsyuk, S., Schreiber, A., Thomas, R., 2009a. Nyerereite and nahcolite inclusions in diamond: evidence for lower-mantle carbonatitic magmas. Mineralogical Magazine 73, 797–816. doi:10.1180/minmag.2009.073.5.797

Kaminsky, F., Zakharchenko, O., Davies, R., Griffin, W., Khachatryan-Blinova, G., Shiryaev, A., 2001. Superdeep diamonds from the Juina area, Mato Grosso State, Brazil. Contr. Mineral. and Petrol. 140, 734–753. doi:10.1007/s004100000221

Kaminsky, F.V., Kaminsky, F.V., Kaminsky, F.V., McCammon, C.A., Ryabchikov, I.D., Abakumov, A.M., Longo, M., Turner, S., Heidari, H., 2015. Oxidation potential in the Earth's lower mantle as recorded by ferropericlase inclusions in diamond. Earth and Planetary Science Letters 417, 49–56. doi:10.1016/j.epsl.2015.02.029

Kaminsky, F.V., Kaminsky, F.V., Khachatryan, G.K., Andreazza, P., Andreazza, P., Araujo, D., Griffin, W.L., Griffin, W.L., 2009b. Super-deep diamonds from kimberlites in the Juina area, Mato Grosso State, Brazil. Lithos 112, 833–842. doi:10.1016/j.lithos.2009.03.036

Katsura, T., Yoneda, A., Yamazaki, D., Yoshino, T., Ito, E., Suetsugu, D., Bina, C., Inoue, T., Wiens, D., Jellinek, M., 2010. Adiabatic temperature profile in the mantle. Physics of the Earth and Planetary Interiors 183, 212–218. doi:10.1016/j.pepi.2010.07.001

Kelemen, P.B., Yogodzinski, G.M., Scholl, D.W., 2003. Along-strike variation in lavas of the Aleutian island arc: Implications for the genesis of high Mg# andesite and the continental crust. Inside the subduction factory. doi:10.1029/2004GC000715/full

Kessel, R., Schmidt, M.W., Schmidt, M.W., Ulmer, P., Pettke, T., 2005. Trace element signature of subduction-zone fluids, melts and supercritical liquids at 120–180 km depth. Nature 437, 724–727. doi:10.1038/nature03971

Kiseeva, E.S., Litasov, K.D., Yaxley, G.M., Ohtani, E., Kamenetsky, V.S., 2013a. Melting and Phase Relations of Carbonated Eclogite at 9-21 GPa and the Petrogenesis of Alkali-Rich Melts in the Deep Mantle. Journal of Petrology 54, 1555–1583. doi:10.1093/petrology/egt023

Kiseeva, E.S., Wood, B.J., Ghosh, S., Stachel, T., 2016. The pyroxenite-diamond connection. Geochemical Perspectives Letters 2, 1–9. doi:10.7185/geochemlet.1601

Kiseeva, E.S., Yaxley, G.M., Stepanov, A.S., Tkalcic, H., Litasov, K.D., Kamenetsky, V.S., 2013b. Metapyroxenite in the mantle transition zone revealed from majorite inclusions in diamonds. Geol 41, 883–886. doi:10.1130/g34311.1

Klemme, S., Blundy, J.D., Wood, B.J., 2002. Experimental constraints on major and trace element partitioning during partial melting of eclogite. Geochimica et Cosmochimica Acta 66, 3109–3123. doi:10.1016/S0016-7037(02)00859-1

Klemme, S., Meyer, H.-P., Meyer, H.P., 2003. Trace element partitioning between baddeleyite and carbonatite melt at high pressures and high temperatures. Chemical Geology 199, 233–242. doi:10.1016/S0009-2541(03)00081-0

Klimm, K., Klimm, K., Blundy, J.D., Green, T.H., 2008. Trace Element Partitioning and Accessory Phase Saturation during H2O-Saturated Melting of Basalt with Implications for Subduction Zone Chemical Fluxes. Journal of Petrology 49, 523–553. doi:10.1093/petrology/egn001

Kopylova, M.G., Gurney, J.J., Daniels, L.R.M., 1997. Mineral inclusions in diamonds from the River Ranch kimberlite,

Zimbabwe. Contr. Mineral. and Petrol. 129, 366–384. doi:10.1007/s004100050343
Liebske, C., Corgne, A., Frost, D.J., Rubie, D.C., Wood, B.J., 2005. Compositional effects on element partitioning between Mg-silicate perovskite and silicate melts. CMP 149, 113–128. doi:10.1007/s00410-004-0641-8
McDonough, W.F., 2001. The composition of the earth, International Geophysics, International Geophysics. Elsevier. doi:10.1016/s0074-6142(01)80077-2
Moore, R.O., Gurney, J.J., Griffin, W.L., Shimizu, N., 1991. Ultra-high pressure garnet inclusions in Monastery diamonds: trace element abundance patterns and conditions of origin. Eur.J.Mineral. 3, 213–230. doi:10.1127/ejm/3/2/0213
Ohta, A., Ishii, S., Sakakibara, M., Mizuno, A., Kawabe, I., 1999. Systematic correlation of the Ce anomaly with the Co/(Ni+Cu) ratio and Y fractionation from Ho in distinct types of Pacific deep-sea nodules. GEOCHEMICAL JOURNAL 33, 399–417. doi:10.2343/geochemj.33.399
Pertermann, M., Hirschmann, M.M., Hametner, K., Günther, D., Schmidt, M.W., 2004. Experimental determination of trace element partitioning between garnet and silica-rich liquid during anhydrous partial melting of MORB-like eclogite. Geochem. Geophys. Geosyst. 5, n/a–n/a. doi:10.1029/2003GC000638
Philpotts, J.A., Schnetzler, C.C., 1968. Europium anomalies and the genesis of basalt. Chemical Geology 3, 5–13. doi:10.1016/0009-2541(68)90009-0
Salters, V.J.M., Longhi, J.E., Bizimis, M., 2002. Near mantle solidus trace element partitioning at pressures up to 3.4 GPa. Geochem. Geophys. Geosyst. 3, 1–23. doi:10.1029/2001GC000148
Schärer, U., Berndt, J., Deutsch, A., 2011. The genesis of deep-mantle xenocrystic zircon and baddeleyite megacrysts (Mbuji-Mayi kimberlite): trace-element patterns. Eur.J.Mineral. 23, 241–255. doi:10.1127/0935-1221/2011/0023-2088
Shannon, R.D., 1976. Revised effective ionic radii and systematic studies of interatomic distances in halides and chalcogenides. Acta Crystallographica Section A 32, 751–767. doi:10.1107/s0567739476001551
Stachel, T., 2001. Diamonds from the asthenosphere and the transition zone. Eur.J.Mineral. 13, 883–892. doi:10.1127/0935-1221/2001/0013/0883
Stachel, T., Brey, G.P., Harris, J.W., 2005. Inclusions in Sublithospheric Diamonds: Glimpses of Deep Earth. Elements 1, 73–78. doi:10.2113/gselements.1.2.73
Stachel, T., Brey, G.P., Harris, J.W., 2000a. Kankan diamonds (Guinea) I: from the lithosphere down to the transition zone. Contr. Mineral. and Petrol. 140, 1–15. doi:10.1007/s004100000173
Stachel, T., Harris, J.W., Brey, G.P., Joswig, W., 2000b. Kankan diamonds (Guinea) II: lower mantle inclusion parageneses. Contr. Mineral. and Petrol. 140, 16–27. doi:10.1007/s004100000174
Sun, C., Liang, Y., 2013. The importance of crystal chemistry on REE partitioning between mantle minerals (garnet, clinopyroxene, orthopyroxene, and olivine) and basaltic melts. Chemical Geology 358, 23–36. doi:10.1016/j.chemgeo.2013.08.045
Suzuki, T., Hirata, T., Yokoyama, T.D., Imai, T., Takahashi, E., 2012. Pressure effect on element partitioning between minerals and silicate melt: Melting experiments on basalt up to 20GPa. Physics of the Earth and Planetary Interiors 208-209, 59–73. doi:10.1016/j.pepi.2012.07.008
Sweeney, R.J., Prozesky, V., Przybylowicz, W., 1995. Selected trace and minor element partitioning between peridotite minerals and carbonatite melts at 18-46 kb pressure. Geochimica et Cosmochimica Acta 59, 3671–3683. doi:10.1016/0016-7037(95)00270-A
Tappert, R., Stachel, T., Harris, J.W., Muehlenbachs, K., Ludwig, T., Brey, G.P., 2005. Subducting oceanic crust: The source of deep diamonds. Geol 33, 565. doi:10.1130/g21637.1
Taura, H., Yurimoto, H., Kato, T., Sueno, S., 2001. Trace element partitioning between silicate perovskites and ultracalcic melt. Physics of the Earth and Planetary Interiors 124, 25–32. doi:10.1016/S0031-9201(00)00221-1
Thomson, A.R., EIMF, Kohn, S.C., Bulanova, G.P., Smith, C.B., Araujo, D., Walter, M.J., 2014. Origin of sub-lithospheric diamonds from the Juina-5 kimberlite (Brazil): constraints from carbon isotopes and inclusion compositions. Contr. Mineral. and Petrol. 168. doi:10.1007/s00410-014-1081-8
Thomson, A.R., Walter, M.J., Kohn, S.C., Brooker, R.A., 2016. Slab melting as a barrier to deep carbon subduction. Nature 529, 76–79. doi:10.1038/nature16174
Toyoda, K., Nakamura, Y., Masuda, A., 1990. Rare earth elements of Pacific pelagic sediments. Geochimica et Cosmochimica Acta 54, 1093–1103. doi:10.1016/0016-7037(90)90441-M
Tuff, J., Gibson, S.A., 2007. Trace-element partitioning between garnet, clinopyroxene and Fe-rich picritic melts at 3 to 7 GPa. Contr. Mineral. and Petrol. 153, 369–387. doi:10.1007/s00410-006-0152-x
van Orman, J.A., Grove, T.L., Shimizu, N., 2002. Rare earth element diffusion in a natural pyrope single crystal at 2.8 GPa. Contributions to Mineralogy and Petrology 142, 416–424. doi:10.1007/s004100100304
van Westrenen, W., Blundy, J., Wood, B., 1999. Crystal-chemical controls on trace element partitioning between garnet and anhydrous silicate melt. American Mineralogist 84, 838–847. doi:10.2138/am-1999-5-617
van Westrenen, W., Blundy, J.D., Wood, B.J., 2000. Effect of Fe^{2+} on garnet–melt trace element partitioning: experiments in FCMAS and quantification of crystal-chemical controls in natural systems. Lithos 53, 189–201. doi:10.1016/S0024-4937(00)00024-4
van Westrenen, W., Draper, D.S., 2007. Quantifying garnet-melt trace element partitioning using lattice-strain theory: new crystal-chemical and thermodynamic constraints. Contr. Mineral. and Petrol. 154, 717–730.

doi:10.1007/s00410-007-0222-8
van Westrenen, W., Wood, B.J., Blundy, J.D., 2001. A predictive thermodynamic model of garnet–melt trace element partitioning. Contr. Mineral. and Petrol. 142, 219–234. doi:10.1007/s004100100285
Walter, M.J., Bulanova, G.P., Armstrong, L.S., Keshav, S., 2008. Primary carbonatite melt from deeply subducted oceanic crust. Nature 454, 622–625. doi:10.1038/nature07132
Walter, M.J., Kohn, S.C., Araujo, D., Bulanova, G.P., Smith, C.B., Gaillou, E., Wang, J., Steele, A., Shirey, S.B., 2011. Deep Mantle Cycling of Oceanic Crust: Evidence from Diamonds and Their Mineral Inclusions. Science 334, 54–57. doi:10.1126/science.1209300
Walter, M.J., Nakamura, E., Trønnes, R.G., Frost, D.J., 2004. Experimental constraints on crystallization differentiation in a deep magma ocean. Geochimica et Cosmochimica Acta 68, 4267–4284. doi:10.1016/j.gca.2004.03.014
Wilding, M.C., 1990. Study of diamonds with syngenetic inclusions. Edinburgh.
Wirth, R., Dobrzhinetskaya, L., Harte, B., Schreiber, A., Green, H.W., 2014. High-Fe (Mg,Fe)O inclusion in diamond apparently from the lowermost mantle. Earth and Planetary Science Letters 404, 365–375. doi:10.1016/j.epsl.2014.08.010
Zedgenizov, D.A., Shatskiy, A., Ragozin, A.L., KAGI, H., Shatsky, V.S., 2014. Merwinite in diamond from São Luiz, Brazil: A new mineral of the Ca-rich mantle environment. Am. Min. 99, 547–550. doi:10.1515/am.2014.4767
Zhang, J., Herzberg, C., 1994. Melting experiments on anhydrous peridotite KLB-1 from 5.0 to 22.5 GPa. J. Geophys. Res. 99, 17729. doi:10.1029/94jb01406

FIGURE CAPTIONS

Figure 1: Mineral/melt parition coefficients for bridgmanite collated from the literature H04, Hirose et al. (2004); W04, Walter et al (2004); C05, Corgne et al. (2005); T01, Taura et al. (2001); L05, Liebske et al. (2005) and the lattice strain model used throughout this study as described in the text.

Figure 2: Mineral/melt parition coefficients for calcium silicate perovskite collated from the literature AKW[unpublished], unpublished data from LS Armstrong, S Keshav and MJ Walter; D09, Dalou et al. (2009); C02, Corgne et al. (2002); H04, Hirose et al. (2004) and the lattice strain model used throughout this study as described in the text.

Figure 3: Fitted D_0 (equation 5) vs lattice strain model for 3+ cations in garnet as described.

Figure 4: Bulk silicate earth normalised McDonough (2001) spider diagrams of Juina-5 **(a)** former 'bridgmanite', **(b)** former 'calcium silicate perovskite', **(c)** majoritic garnet, **(d)** 'NAL' and 'CF phase' inclusions.

Figure 5: Bulk silicate earth normalised McDonough (2001) REE diagrams of Juina-5 **(a)** former 'bridgmanite', **(b)** former 'calcium silicate perovskite', **(c)** majoritic garnet, **(d)** 'NAL' and 'CF phase' inclusions.

Figure 6: BSE normalised trace element composition of **(a)** 'calcium silicate perovskite', **(b)** majoritic garnet, **(c)** 'bridgmanite' inclusions compared with models for subsolidus peridotite in the transition zone (dashed blue), peridotite in the lower mantle (dashed dark green) and MORB in the transition

zone (dashed red) assemblage components as described in the text. D04, Davies et al. (2004); S00, Stachel et al. (2000); K01, Kaminsky et al. (2001); T05, Tappert et al. (2005); B10, Bulanova et al. (2010); H97, Hutchison (1997); M91, Moore et al. (1991); Burnham, Burnham et al., *this issue*. **(d)** BSE normalised trace element patterns of natural carbonatite lavas from the Cape Verde and Canary Islands (Hoernle et al., 2002), compared with the melts calculated to be in equilibrium with majoritic garnet and calcium perovskite inclusions in the Juina-5 diamonds (this study). Equilibrium melts were calculated using the partition coefficients for calcium silicate perovskite and metabasic majorite from table 1.

Figure 7: The results from modelling source rock compositions for 'calcium silicate perovskite' inclusions **(a)** Ju5-115c **and (b)** Ju5-82. The reported inclusion composition is the upper blue line and the red line is the melt in equilibrium with this inclusion surrounded by 95 % confidence intervals. The green curve is the calculated source rock, which can be compared with the composition of ALL-MORB (Gale et al., 2013) and/or "processed MORB", the black dotted and solid lines respectively. Details of modelling are described in the text.

Figure 8: (a) Ca (per formula unit) plotted against Sm/Lu (BSE normalised), coloured by calculated pressure, for global majoritic garnet inclusions. **(b)** Calculated melts in equilibrium with all majoritic inclusions using partition coefficients specific to each inclusion composition, from a lattice strain model (equation 1) using r_0, E and D_0 calculated using equations 2, 3 and 5. The pressure of each inclusion was calculated from its chemistry using the barometer presented by Beyer (2015) and the temperature of inclusion formation was assumed to be 1600 °C for all samples.

Figure 9: (a) fractional crystallisation model where majoritic garnet and calcium perovskite are removed from the melt in a 10:1 mass ratio **(b)** only calcium perovskite is removed from the melt in each model step. The bold black curve is the most most enriched 'calcium perovskite', which is used as the model's starting point. The green lines are other Juina-5 'calcium silicate perovskite' inclusions. The red lines are Juina-5 majoritic garnet inclusions. The light grey lines are literature majoritic garnet inclusions. The pink dashed lines are calcium perovskite minerals produced in the model crystallisation sequence; in **(a)** after 160 model steps and **(b)** after 85 and 200 model steps. The light blue line is the majorite in equilibrium with the initial melt composition. The bold dark blue solid line is the majoritic garnet produced after 115 model steps in both models. The various other blues lines in **(b)** demonstrate the effects of varying pressure and temperature on the composition of crystallising majoritic garnet.

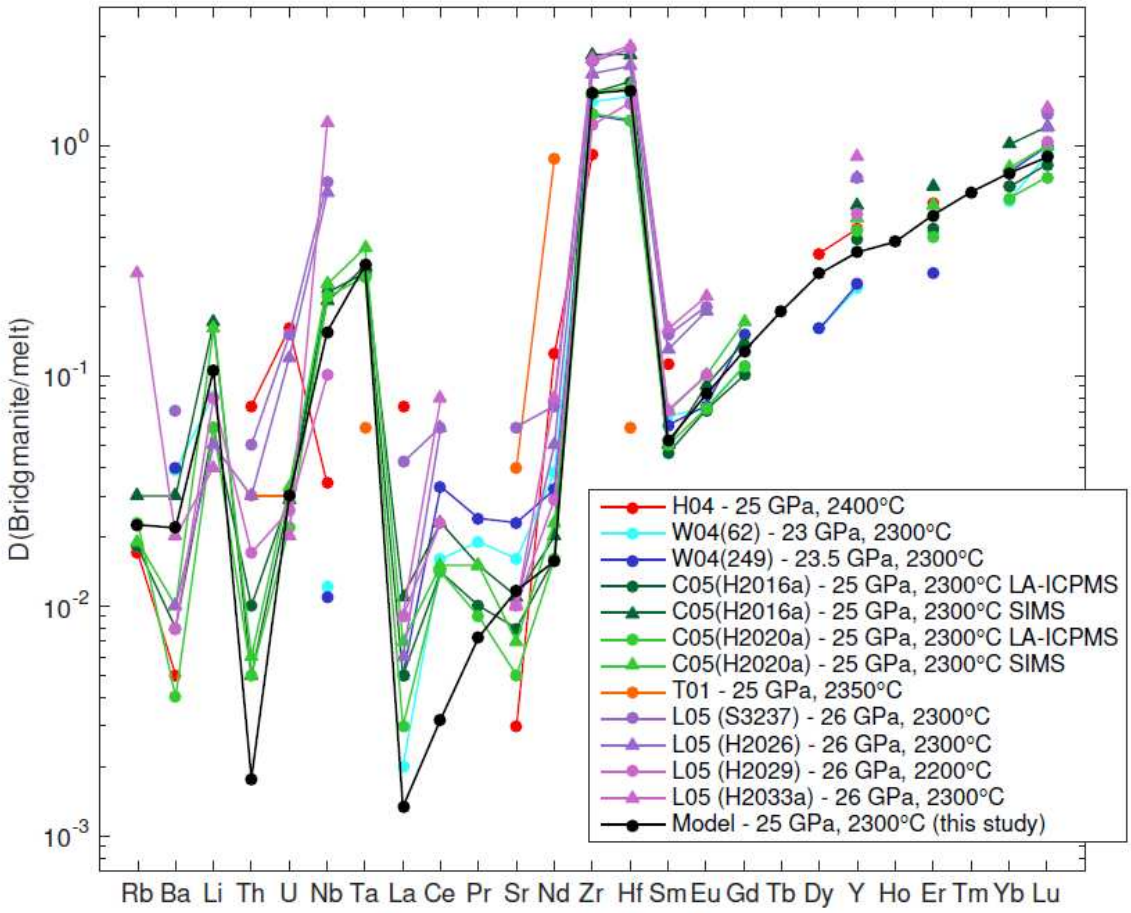

Figure 1

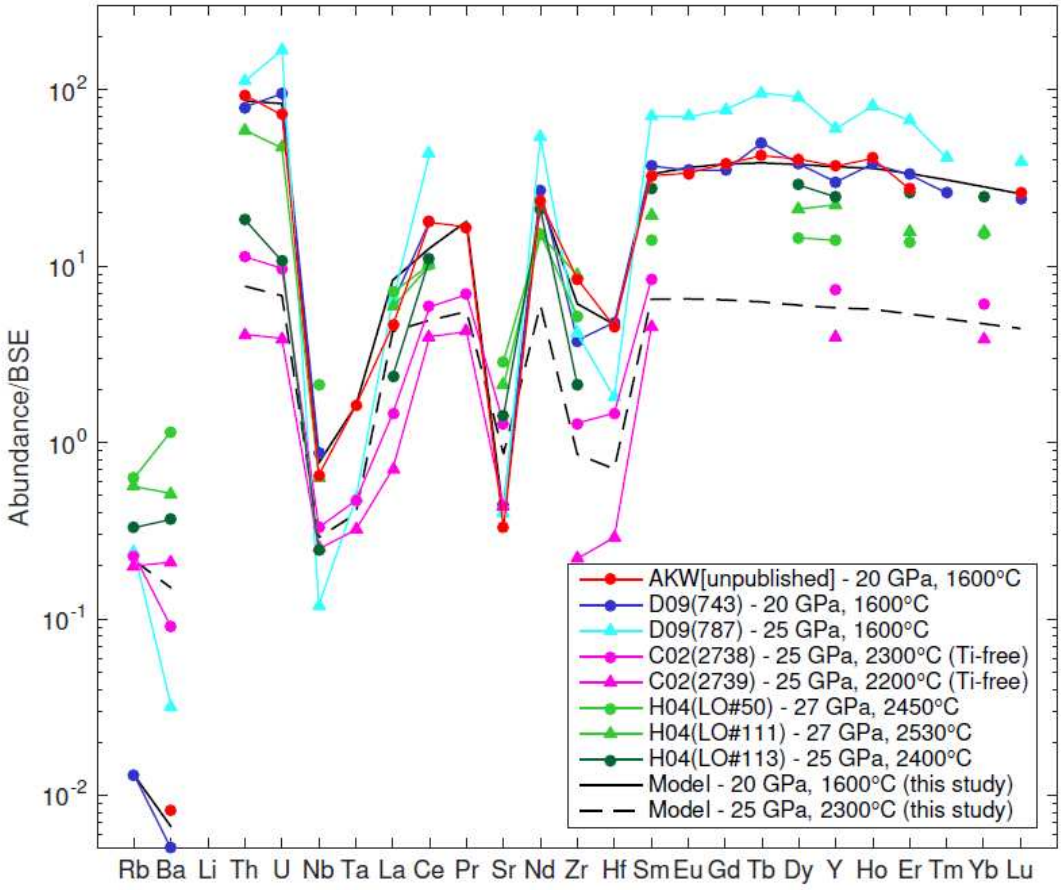

Figure 2

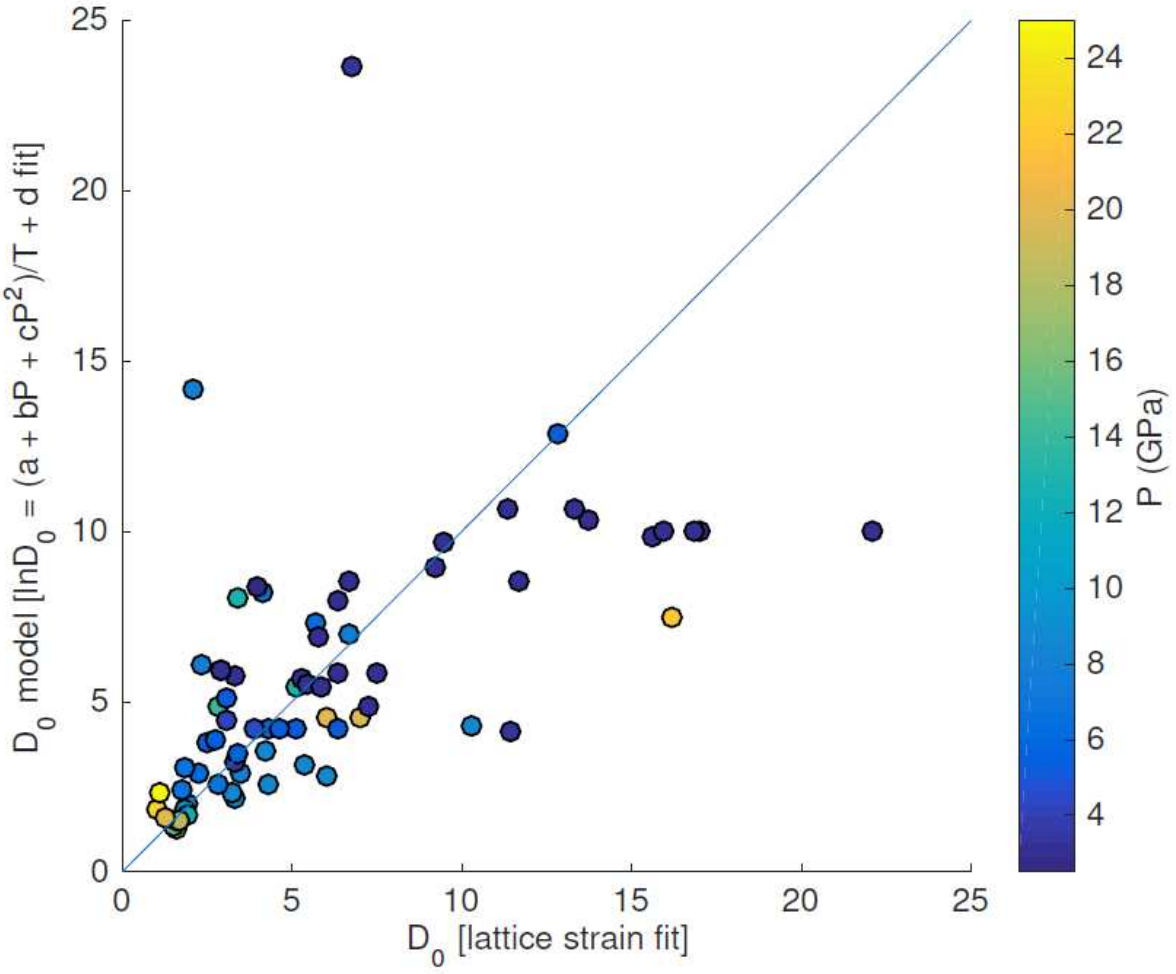

Figure 3

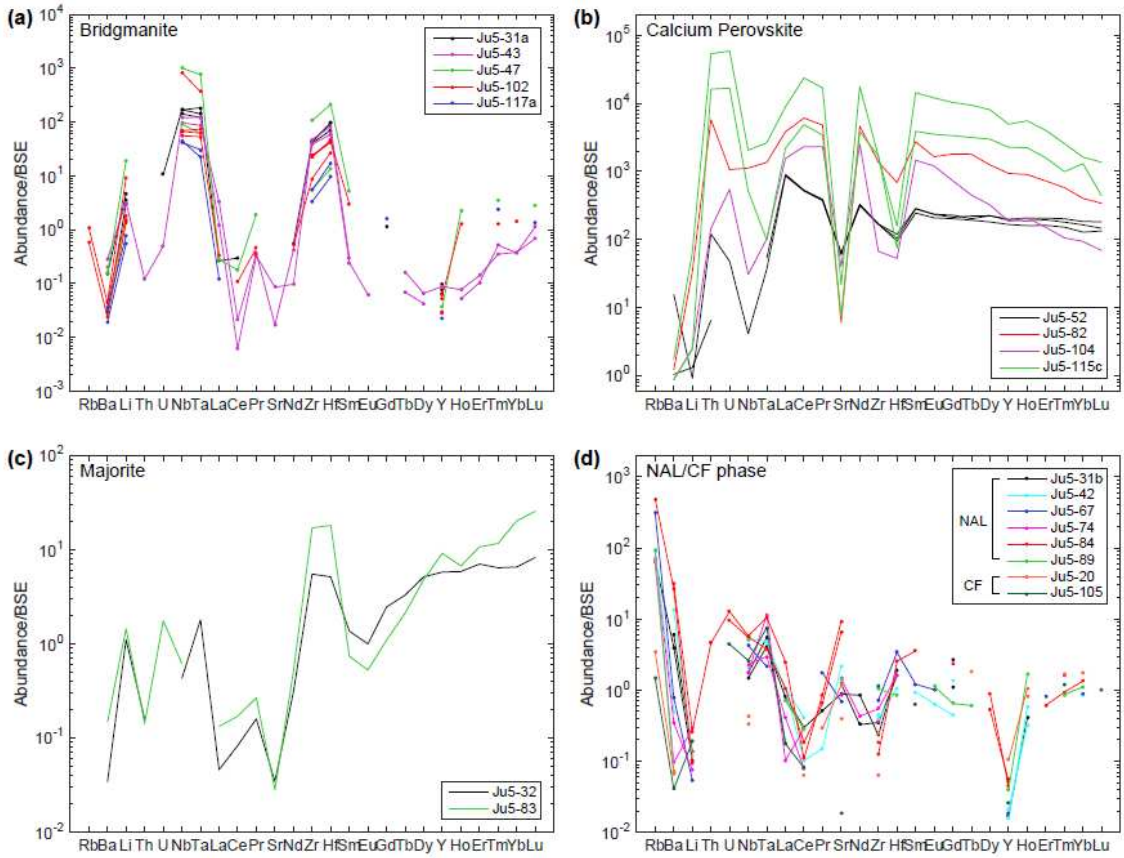

Figure 4

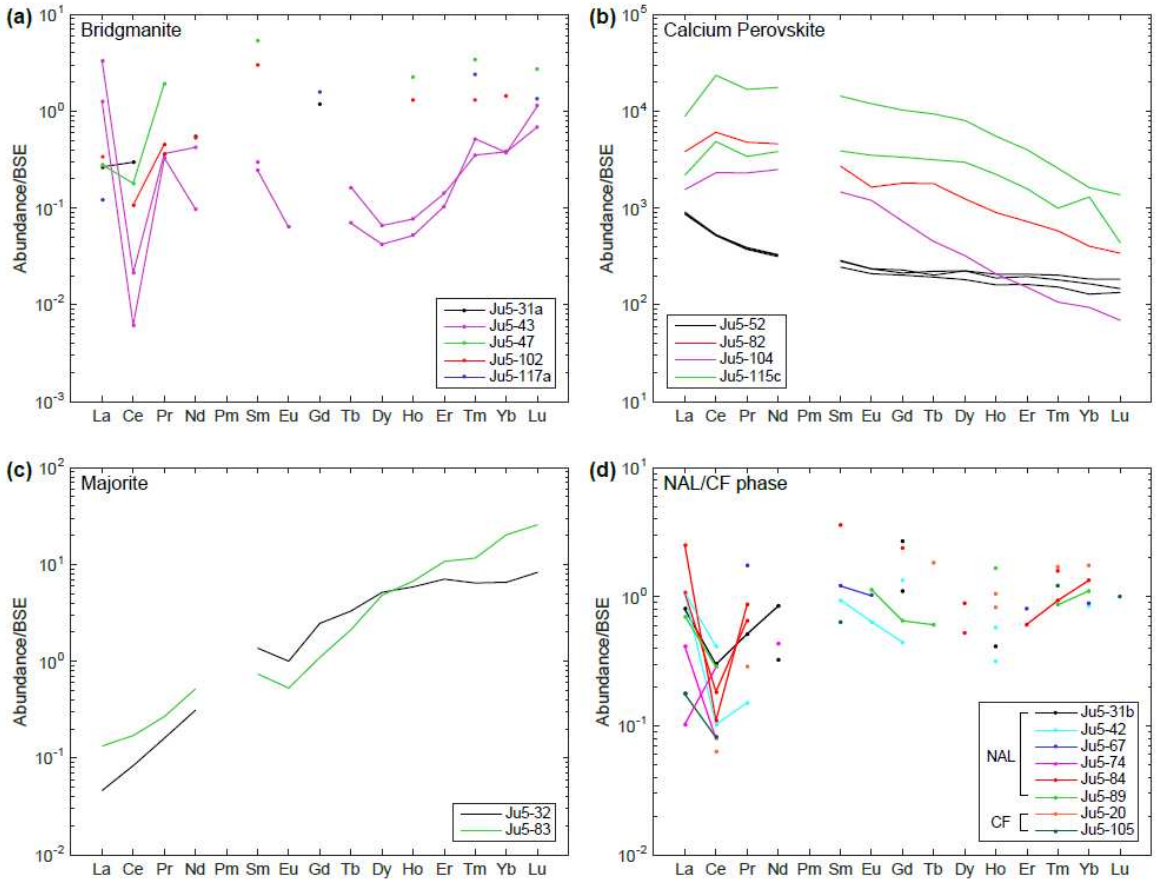

Figure 5

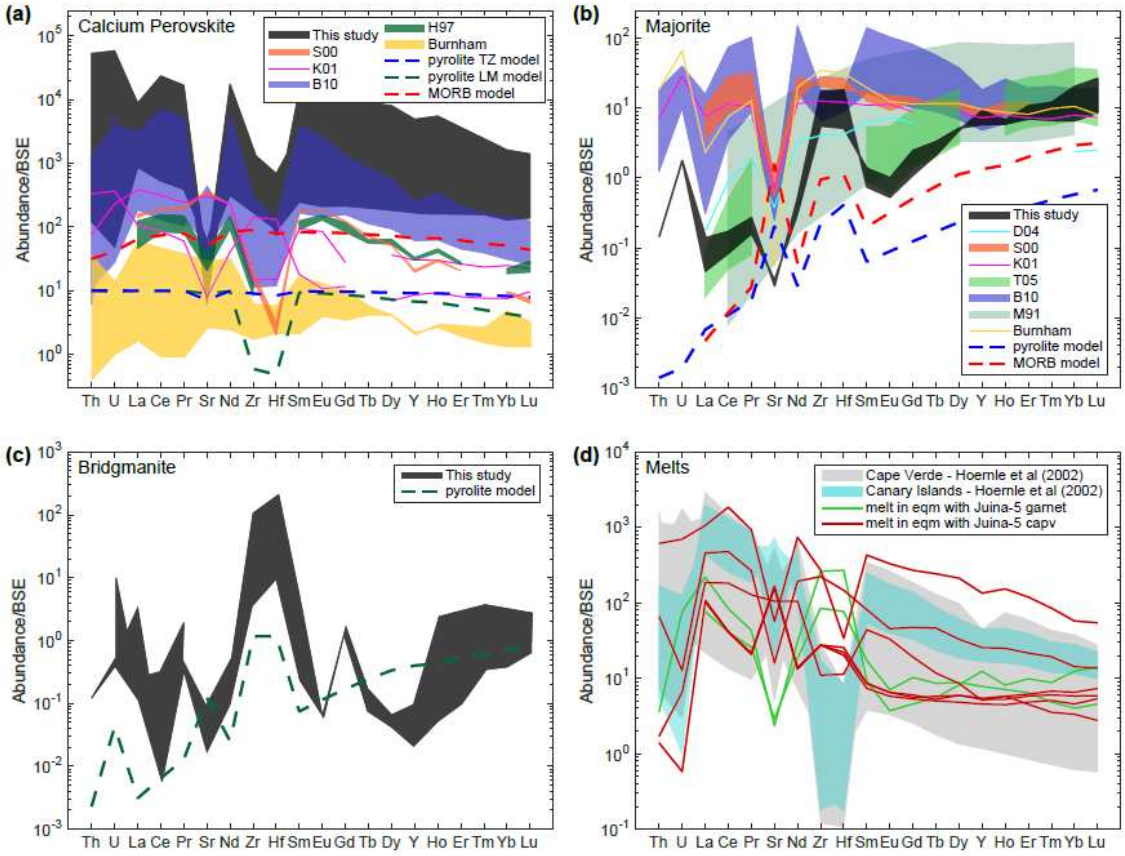

Figure 6

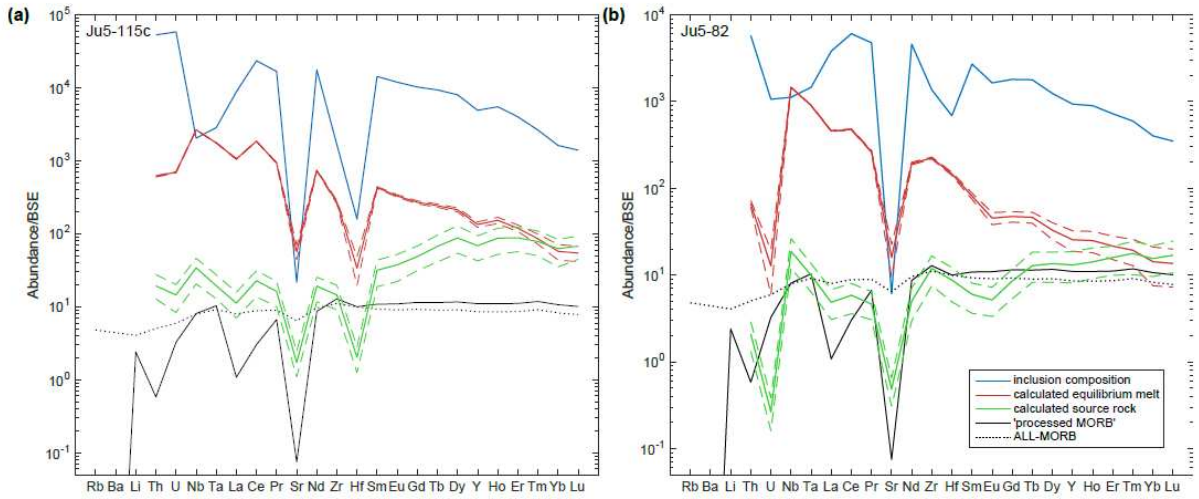

Figure 7

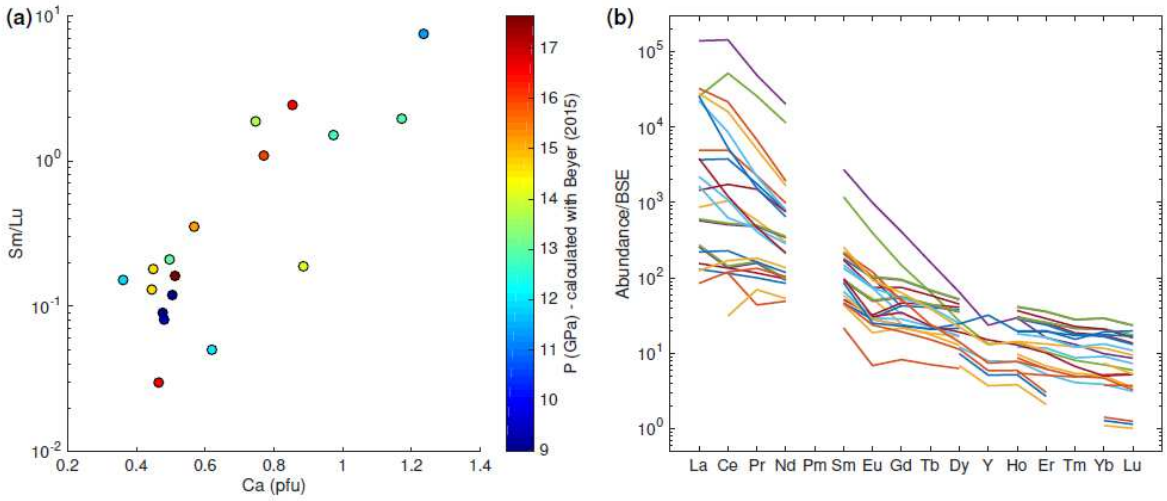

Figure 8

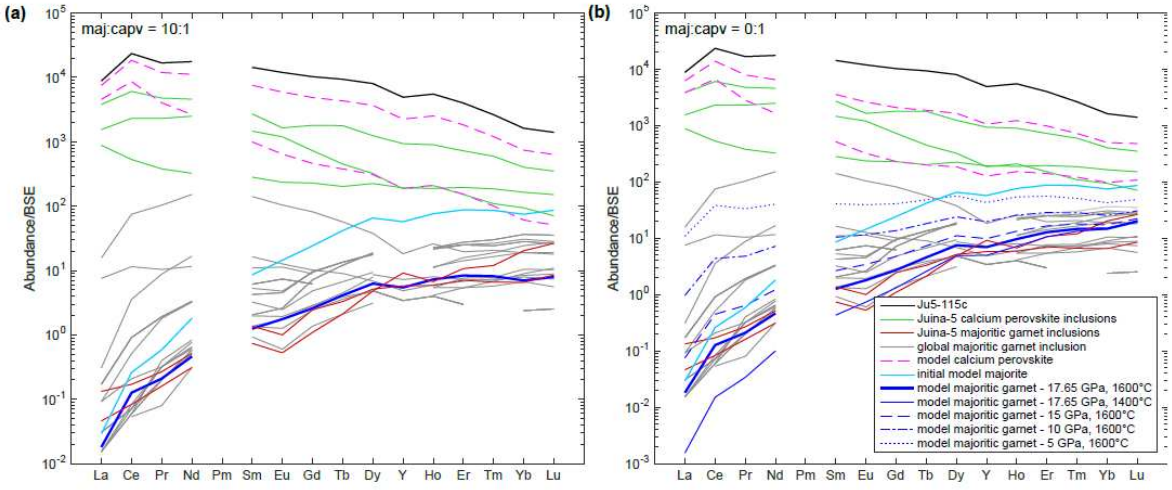

Figure 9

Table 1

Phase	**Calcium silicate perovskite**	**Calcium silicate perovskite**	**Magnesium silicate perovskite**	**Peridotitic majoritic garnet**	**Metabasic majoritic garnet**	**Peridotitic clinopyroxene**		**Eclogitic clinopyroxene**		**Olivine**		**Ferropericlase**	**Magnesite**	**Stishovite**
Reference	this study (Dalou et al. 2009 and Keshav et al. unpublished)	this study (Corgne et al. 2002 average)	this study (Walter et al. 2004 and Corgne et al. 2005)	Corgne et al. (2012) converted to 1600 °C	Suzuki et al. (2012) converted to 1600 °C	Dasgupta et al. (2009)		Suzuki et al. (2012)		Dasgupta et al. (2009)		Walter et al. (2004)	Dasgupta et al. (2009)	This study
P (GPa)	20	25	25	15	15	8.6		15		-		25	8.6	-
T (°C)	1600	2250	2300	1600	1600	1470		2000		-		2300	1470	-
3+														

D_0	38.51		3.05	*3.109#*	*3.109#*							0.05		
E	400.17		410.54	678.91	519.50							164.40		
r_0	1.04		0.84	0.92	0.91							0.98		
4+														
D_0	89.81		1.76											
E	340.53		762.32											
r_0	1.03		0.82											
Rb	0.0130	0.2150	0.0225	0.0920	0.0055	0.0030	*AG01*	0.0030	*AG01*	0		0.5	0.0105	0.0001
Ba	0.0066	0.1500	0.0218	0.0460	0.0001	0.0080	*AG01*	0.0080	*AG01*	0.000000001	*K03*	0.64	0.0110	0.0001
Li			0.1064	0.0630	0.2300	0.0000		0.8800		0		0.5	0.0100	0.0001
Th	86.6373	7.6974	0.0018	0.0120	0.0400	0.0020		0.0022	*K[u*	0.000000	*K03*	0	0.0031	0.0001

									p]	001				
U	83.4665	6.8050	0.0299	0.0160	0.0230	0.0010		0.0020	*K[up]*	0.000000001	*K03*	0	0.0015	0.0001
Nb	0.7683	0.2900	0.1555	0.0120	0.0100	0.0010		0.0003	*K[up]*	0		0.002	0.0015	0.0001
Ta	1.6202	0.3950	0.3025	0.0140	0.0060	0.0020		0.0007	*K[up]*	0		0.002	0.0020	0.0001
La	8.3315	4.2698	0.0013	0.0056	0.0006	0.0060		0.0180		0.000007		0.017823613	0.0041	0.0001
Ce	12.6667	4.9346	0.0032	0.0140	0.0020	0.0120		0.0280		0.00001		0.021637074	0.0036	0.0001
Pr	17.9568	5.5313	0.0073	0.0321	0.0062	0.0225	*	0.0480		0.00004		0.025696739	0.0055	0.0001
Sr	0.3836	0.8600	0.0117	0.0110	0.0120	0.0300	*D09*	0.0960		0.02	*S95*	0	0.0485	0.0001

Nd	23.7822	6.0155	0.0156	0.0683	0.0170	0.0330		0.0600		0.00007		0.029873242	0.0070	0.0001
Zr	6.1194	0.8577	1.6900	0.1500	0.0650	0.0240		0.0400		0.036	*S95*	0.15	0.0080	0.0001
Hf	4.6768	0.7093	1.7454	0.2300	0.0670	0.0630		0.0740		0.036	*S95*	0.076	0.0060	0.0001
Sm	33.2705	6.4895	0.0519	0.2161	0.0797	0.0530		0.1100		0.0007	*K03*	0.037054011	0.0125	0.0001
Eu	36.1927	6.5216	0.0827	0.3321	0.1420	0.0700		0.1100		0.00095	*K03*	0.039901395	0.0198	0.0001
Gd	37.9857	6.4470	0.1278	0.4900	0.2400	0.0900		0.1400		0.0012	*K03*	0.042484374	0.0110	0.0001
Tb	38.4969	6.2719	0.1914	0.6948	0.3848	0.1050	*	0.1600		0.0026	*	0.044737286	0.0300	0.0001
Dy	37.7060	6.0069	0.2781	0.9476	0.5862	0.1200		0.2000		0.004	*K03*	0.046603688	0.0370	0.0001

Y	36.6149	5.8051	0.3448	1.1255	0.7407	0.1300		0.2000		0.023	*K03*	0.047540182	0.0523	0.0001
Ho	35.9133	5.6947	0.3823	1.2200	0.8267	0.1400	*	0.2100		0.016	*	0.047944518	0.0550	0.0001
Er	33.5193	5.3630	0.5007	1.4955	1.0922	0.1500		0.2100		0.009	*K03*	0.048829053	0.0705	0.0001
Tm	30.8662	5.0331	0.6287	1.7593	1.3653	0.1550	*	0.2300		0.016	*	0.049336834	0.0900	0.0001
Yb	28.2107	4.7199	0.7608	1.9996	1.6296	0.1600		0.2300		0.023	*K03*	0.049549531	0.1135	0.0001
Lu	25.7246	4.4335	0.8913	2.2090	1.8719	0.1700		0.2400		0.03	*K03*	0.049545131	0.1375	0.0001

Data from alternative sources - AG01, Adam and Green (2001); D09, Dasgupta et al (2009) 6.6 GPa experiment; K03, Kelemen (2003); S95, Sweeney (1995); K[up], Keshav (unpublished) *interpolated from adjacent elements in this study. #Fixed using Equation 5.

Table 2

Sample	Ju5-20	20	Ju5-31a	Ju5-31a	Ju5-31a	Ju5-31b	Ju5-31b	Ju5-32	Ju5-42	Ju5-43	Ju5-43	Ju5-43	Ju5-47	Ju5-47	Ju5-52	Ju5-52	Ju5-52	Ju5-67	Ju5-73a	Ju5-74	Ju5-74	Ju5-82	Ju5-83	84	Ju5-84	Ju5-89	Ju5-90	Ju5-2	Ju5-2	Ju5-2	Ju5-2	Ju5-4	Ju5-5	Ju5-5c	Ju5-5c	Ju5-6a	Ju5-6a	Ju5-7a	Ju5-7a	Ju5-9	Ju5-9
mineral			MgPv	MgPv	MgPv	NAL	NAL	Major te garnet	NAL	NMgPv	MgPv	MgPv	MgPv	MgPv	CaPv	CaPv	CaPv	NAL	olivine	NAL	NAL	CaPv	Major te garnet	NAL	NAL	NAL	SiO2	SiO2	MgPv	MgPv	MgPv	MgPv	CaPv	CaPv	CaPv	cpx	cpx	MgPv	MgPv	garnet	garnet
phase	CF	CF	v	v	v	L	AL	garnet	L	AL	v	v	v	v	v	Pv	Pv	Pv	L	e	L	L	Pv	garnet	AL	L	L	2	2	v	v	v	v	Pv	CF	Pv	Pv	x	x	v	v	et	et
Rb	2.1					39.9			57.3	10.1								18 8.2	1.0	42.6	36.9			29 3.8	54.3					0.6	0.3		0.9						0.2	0.4
Ba	0.5	4	0.42			1.0	0.4	0.2	8.3	3.8	41.9	1.4	1.3	0.1	1.0	7.1	4.2	5.2	5.2		2.3	0.6	8.1	1.0	20 4.5	17 5.9	0.5	0.5		0.3	0.3	2.8	5.3	11.7	5.9	0.6	1.4	0.1	0.2	0.4	0.4
Th								0.0			0.1				0.9	0.1						0.4	6	0.0	0.1							1.1	4.2	1.2						

												0				5	7	4					1.0		4								.8		48.	86.						
																																			3	8						
																																			11							
					0.						0.	0.					1.						21.		0.	0.		0.					10	0.	66.	33						
U					2						4	0					0						3	0.0	3	2		7					.9	1	5	2.4						
				11	11						20				66															55					13							
		0.	93	2.	1.	1.	1.		3.	1.	5.	64	79	60	5.		2.		2.		1.	1.	73		3.	3.	3.		44	1.	45	36	20	1.	48.	34			30	27	0.	0.
Nb	0.3	2	.6	0	0	1	0	0.3	6	4	4	.4	.1	.7	3		8		8		5	2	9.6	0.4	8	7	3		.4	3	.7	.8	.4	7	1	1.8			.0	.6	1	2
			4.	5.	7.	0.	0.		0.		13	3.	4.	2.	30	2.	1.		0.		0.	0.	54.		0.	0.			2.	14	3.	2.	4.	0.	10				0.	1.	0.	0.
Ta			9	7	4	2	2	0.1	2		.5	5	9	5	.4	1	5		1		1	5	1		4	2			5	.7	0	1	1	3	5.6	4.0			9	2	6	5
																57	56	58					24										10		57	14						
					0.	0.	0.		0.	0.	29	2.	0.		0.	3.	1.	9.		0.	0.	0.	79.		1.	0.	0.					0.	05	0.	33.	14.	0.	1.	0.		0.	0.
La					2	1	5	0.0	7	7	.5	1	8		2	7	6	7		1	3	1	2	0.1	6	7	5					2	.3	1	3	2	9	0	1		1	1
																89	86	88					10										38		39	81						
					0.		0.		0.	0.	0.	0.	0.		0.	0.	9.	3.			0.	0.	17		0.	0.	0.			0.			84	0.	45	49.	1.	2.			1.	1.
Ce	0.1				5		5	0.1	2	7	5	0	0		3	8	4	8			1	5	3.4	0.3	2	3	5			2			.7	1	4.7	1	8	2			8	8

																						11									57		41							
		0.					0.		0.		1.	0.	0.		0.	94	93	97	0.			93.		0.	0.			0.	0.		5.		93.	85					0.	0.
Pr		1					1	0.0	0		7	1	1		5	.9	.2	.5	4			4	0.1	2	2			1	1		5		4	1.3					8	7
						2			4							12	12	12						18	13						80									
		23				4.	17		4.	24	6.	0.	1.			82	22	07	13	29	16	12		7.	1.	27					7.	0.	43	15	70	72			3.	3.
Sr	7.9	.7				5	.7	0.7	2	.0	3	3	7			.5	.4	.7	.8	.1	.7	2.1	0.6	9	4	.9					6	4	4.5	2.2	.8	.5			3	3
																40	39	41				57									31		21	47						
					0.	0.	1.				6.	0.	0.			5.	2.	1.		0.		43.								0.	19		99	91.					8.	9.
Nd					7	4	1	0.4			5	5	1			3	7	1		5		5	0.6							7	.6		6.1	7					0	6
			42	45	46						61	40	49		11	17	17	17				14					25	24	23		70		17	17					13	13
		2.	4.	2.	0.	3.	2.		4.	4.	7.	7.	6.	59	16	58	76	72	7.	5.	3.	35		1.	2.	10	0.	7.	3.	93	8.	12	44	63	1.	1.	57	34	5.	4.
Zr	0.7	6	1	6	8	7	4	57.9	1	8	2	8	8	.2	.7	.9	.4	.0	6	7	8	2.9	179.1	3	0	.9	0	6	7	.2	0	.2	5.0	2.5	7	7	.2	.9	3	2
			19	26	26	0.	0.		0.		27	16	23	3.	60	29	26	33	1.	0.		19		0.		0.	11	12	13	7.	14		44.	20.			4.	2.	3.	3.
Hf			.9	.6	.7	5	5	1.4	3		.8	.6	.1	8	.0	.1	.5	.5	0	5		2.3	5.1	7		2	.9	.1	.0	7	.8		5	9			9	7	9	9
																11	10	11				11									59		58	15						
										0.		0.	0.		2.	5.	0.	7.	0.			11.		1.				1.			9.	0.	68.	91.					5.	5.
Sm								0.6		4		1	1		2	6	6	6	5			6	0.3	5				3			5	3	0	7					4	5

Eu								0.2		0.1		0.0			35.3	31.4	35.2	0.2		246.5	0.1			0.2					179.6		1791.8	525.0		2.0	1.9
Gd					0.6	0.6	1.5	1.3	0.7	0.2	9.5	0.3	0.1		123.4	109.4	114.9			972.6	0.6	1.3		0.4					393.0		5539.6	1807.0	0.8		
Tb	0.2							0.3			0.1	0.0	0.0		20.2	19.3	22.2			178.2	0.2			0.1					45.1		935.7	315.1		1.8	2.1
Dy								3.5				0.0	0.0		150.3	121.8	150.0			831.9	3.2	0.6	0.4						215.8		5377.2	1988.1		13.6	12.9
Y		0.4	0.3	0.3	0.4	0.1	0.2	24.9	0.1	0.1	2.7	0.4		0.2	828.1	717.1	857.4	0.1	0.2	4020.9	39.4	0.2	0.2	0.2	0.2	0.1	0.3	0.1	801.0	0.1	21150.6	9711.4	0.1	88.5	87.7
Ho	0.1	0.2				0.1		0.9	0.0	0.1		0.0	0.0	0.3	28.3	24.1	31.1		0.1	134.7	1.0			0.2			0.2		31.3		826.2	333.8		2.8	3.1

Er								3.1				0.1	0.0			86.0	71.4	90.9	0.4				318.7	4.7	0.3									66.7		1759.7	695.1					9.8	9.3
Tm		0.1						0.5				0.0	0.0		0.2	12.6	10.7	14.2					40.6	0.8	0.1	0.1	0.1					0.1		7.4	0.1	179.0	69.6			0.2		1.4	1.6
Yb	0.8							2.9		0.4	1.0	0.2	0.2			72.4	56.6	81.1	0.4				177.2	8.9	0.6		0.5				0.6			41.4		713.8	571.9					10.1	10.1
Lu								0.6				0.0	0.1		0.2	10.3	9.4	12.8					23.8	1.8										4.8	0.1	95.3	30.6			0.1		1.5	1.5
Sc	14.5	3.9	182.1	183.1	193.3	32.4	21.4	31.9	8.2	6.5	58.9	82.7		82.2	238.1	73.3	68.9	68.9	11.0	5.9	15.7	12.4	23.6	78.5	5.9	1.3	19.4	2.9	2.9	109.5	92.3	104.6	65.4	29.0	12.9	32.0	23.2	1.7	3.4	119.1	95.3	92.4	92.4
Li			4.9	5.7	7.4	0.2	0.2	1.8	0.2		13.5	5.1		2.5	30.4	2.1	1.5		0.1		0.1	0.5	54.1	2.3	0.4	0.2				2.5	14.7	3.0	2.1	4.1	0.3	105.6	4.0			0.9	1.2	0.6	0.5
P	16.0	1.6	3.5	3.1	6.5		127.	409.6		26.3	19.3	875.		9.2	10.9		1.0		494.	2.0	131.	161.	0.5	843.1		81.6	108.			2.7	5.9	6.7	8.6	0.2	103.	0.5	0.4	17.7	17.0	1.4	1.9	1.9	1.9

					8				3						6		0	1				3								6								
							78	22	53	45	42		13								46				25	21	22	22							26	20		
	23	67	11	10	13	8.		9.	16	9.	9.	9.	27	45	30	11	52	5.	11	16.		05	10	2.	8.	8.	6.	6.	6.	23	42		13.	1.	3.	3.	7.	62	68
V	3.3	.7	.2	.2	.2	6	201.3	3	.4	6	3	0	.8	.5	.8	.9	.2	7	.5	1	258.1	.9	.3	9	6	2	5	3	3	.5	.4	7.7	2	7	4	7	3	.7	.2
	19	25	56	58	72	49		27	43	47	31	32				20		87	10			27	11		75	39	49	45	44	11	92	16		41	39	46	52	40	39
	29.	1.	3.	5.	3.	4.		9.	1.	1.	1.	80	16	17	16	53	11	9.	75	68		2.	30		4.	8.	6.	5.	4.	00	6.	92.	13	1.	1.	9.	5.	2.	6.
Cr	4	0	5	9	2	0	1188.8	1	1	3	8	.1	.1	.6	.1	.6	.9	9	.0	6.8	271.4	7	.3		3	8	0	1	5	.8	6	9	5.7	3	1	4	8	6	0
	26	20	31	30	36	31		49	53	62	25	65	17	32	10	23	14	13	15			18	22		12	24	26	25	28	51	11	29		18	21	25	27	22	22
	27.	3.	2.	0.	4.	4.		1.	7.	59	2.	7.	8.	9.	2.	70	19	61	57	70.		49	55	2.	2.	0.	0.	5.	1.	69	27	51.	58	0.	7.	3.	3.	3.	7.
Mn	3	7	3	1	1	3	2232.1	7	3	.0	6	5	8	8	6	.4	.3	.3	.4	7	5311.5	.9	.1	9	9	2	7	8	1	.1	.1	2	4.5	4	5	4	2	3	7
	12	61	48	48	51	63		70	12		35	71	49	47	48	34	41	19	25			60	28		17	30	36	36	38		33				10	25	27	29	29
	64	6.	29	53	55	0.		2.	41	51	20	07	2.	7.	0.	05	5.	84	34	15		3.	28		4.	63	37	33	38	55	82	81.	88.	97	1.	42	07	21	51
Co	0.1	4	.4	.8	.9	4	51.5	2	.7	.2	.6	.6	5	8	8	.8	0	.0	.6	3.2	18.6	3	.1		3	.5	.1	.8	.9	.3	.7	6	2	.8	1	.5	.7	.6	.3
												10					19																						
	31	13	26	22	34	5.		20	56	45	41	8.	1.	5.	1.	68	4.	51	69	18		23	65	1.	0.	38	51	50	56	12	66	26	29.	0.	1.	31	37	91	94
Ga	1.8	.1	.3	.7	.9	0	40.9	.0	.7	.1	.8	6	3	0	3	.6	0	.8	.8	2.0	39.9	.0	.0	5	6	.6	.6	.1	.1	.1	.6	9.1	5	6	7	.6	.3	.6	.2

Mo	633.1	22.6	63.6	57.7	70.2	24.7		120.1	94.8	0.2	25.3	78.9	64.6	63.6	52.9	799.0	3.0	335.4	449.7	51.1		142.2	310.1	9.6	56.9	58.8	63.6	59.2	67.1	235.3	57.4	29.0	34.7	32.1	40.4	46.7	74.5	76.7
Cs	0.2		0.5	0.5	0.7	0.2	0.0	0.1	2.4	0.0	0.5	13.1		0.3	0.2			0.1	0.2	3.1	0.1	0.1	2.2		0.3	0.5	0.3	0.4	1.6	0.4	7.9	0.3		0.2	0.2	0.3		